Effect of the crystallization conditions on the exclusion/inclusion balance in biodegradable poly (butylene succinate-*ran*-butylene adipate) copolymers

Ricardo Arpad Pérez-Camargo[1], Guoming Liu[1,2], Dario Cavallo[3], Dujin Wang[1,2] and Alejandro J Müller[4,5]**

[1] Beijing National Laboratory for Molecular Sciences, CAS Key Laboratory of Engineering Plastics, CAS Research/Education Center for Excellence in Molecular Sciences, Institute of Chemistry, Chinese Academy of Sciences, Beijing 100190, China

[2]. University of Chinese Academy of Sciences, Beijing 100049, China

[3] Department of Chemistry and Industrial Chemistry, University of Genova, Genova, Italy.

[4] POLYMAT and Polymer Sciences and Technology Department, Faculty of Chemistry, University of the Basque Country UPV/EHU, Paseo Manuel de Lardizabal 3, 20018 Donostia-San Sebastián, Spain.

[5] IKERBASQUE, Basque Foundation for Science, 48013, Bilbao, Spain.

ABSTRACT

Biomedical applications of polymers require precise control of the solid-state structure, which is of particular interest for biodegradable copolymers. In this work, we evaluated the influence of crystallization conditions on the comonomer exclusion/inclusion balance of biodegradable poly (butylene succinate-*ran*-butylene adipate) (PBSA) isodimorphic random copolymers. Regardless of the crystallization conditions, the copolymers retain their isodimorphic character displaying a pseudo-eutectic behavior with crystallization in the entire composition range. This illustrates the thermodynamic nature of the isodimorphic behavior for PBSA random copolymers. However, depending on the composition, the crystallization conditions affect the exclusion/inclusion balance of the comonomers. Fast cooling favors BA inclusion inside the PBS crystals, whereas isothermal crystallization strongly limits it. PBA rich compositions behave differently. Both fast and slow crystallization formed the β-phase, whereas BS unit inclusion is favored independently of the cooling conditions. During Successive Self-nucleation and Annealing (SSA), the BA inclusion is intermediate between non-isothermal and isothermal conditions, while the crystalline structure of the PBA phase changes from β-phase to the more stable α-phase. We propose a simple crystallographic model to explain the changes in the unit cell dimension of the copolymers.

Keywords: Isodimorphic biodegradable random copolyesters; Successive-Self-nucleation and Annealing (SSA); crystallization; exclusion/inclusion balance; polymorphism.

1. INTRODUCTION

Random copolymerization is widely employed because it offers the possibility of tailoring the final material properties in between those of the parent components. The advantages of the random copolymerization have been adopted to improve the properties of the most promising bio-based and biodegradable materials, such as poly (lactic acid) (PLA) and poly (butylene succinate) (PBS), among others.[1]

PBS is one of the most promising biodegradable materials since its properties are comparable to commodity non-biodegradable polymers, such as polyethylene (PE) and polypropylene (PP), and its monomers (*i.e.*, 1,4-butanediol and succinic acid) are available from biobased sources.[2, 3] Indeed, it has a relatively high melting temperature (110 °C) that is crucial for applications and is easier to process than other aliphatic polyesters.[2] However, its high crystallinity implies a low degradation rate and barrier properties.[1] The reduction of PBS crystallinity can be achieved by modifying its chain structure or by adding additives and second phases. These modifications include the design of PBS-based chain branched analogs, block and random copolymers, blending with other polymers,[2] incorporating natural fibers,[4] nanocomposites,[5] and others.[1] A recent example of how these modifications affect the PBS properties is the improvement of its barrier properties. The PBS-based copolymers show values comparable or even higher than other materials like low-density polyethylene (LDPE) and poly (lactic acid) that are widely employed in flexible food packaging applications.[6, 7]

The study of random copolymers, and specifically random copolyesters, has attracted the attention of researchers not only for the developed final properties but also for the interesting crystallization modalities, namely: comonomer exclusion, isomorphism, and isodimorphism. Among the different crystallization behaviors, the comonomer exclusion is the most common

case,[8, 9] and its opposite is isomorphism, where the copolymer chains can form a single crystalline phase. So far, only a few cases of isomorphism in copolyesters have been reported.[10-14]

Isodimorphism represents an intermediate case. Let us consider a PA-*ran*-PB random isodimorphic copolymer. It can crystallize in the entire composition range due to the possibility of including comonomeric units of A within the crystal lattice of PB and *vice-versa*. The melting point (T_m) and crystal structure are highly dependent on composition. When T_m is plotted as a function of composition, a clear pseudo-eutectic point is observed. To the left of the pseudo-eutectic point (where PA-rich compositions are located) the copolymer crystallizes with a unit cell that resembles that of the PA homopolymer but with a partial inclusion of B comonomeric units. To the right of the pseudo-eutectic point the converse situation occurs and the copolymer crystallizes with a PB homopolymer type unit cell with a small inclusion of A comonomeric units. At the pseudo-eutectic point, Müller et al. have demonstrated that both PA-rich and PB-rich crystal phases can be formed.[8, 15-22]

As both comonomers are partially included in the crystalline unit cell characteristic of the major component, this is a challenging case study due to the difficulties in predicting the combination of two comonomers that lead to this behavior. Even amongst the known isodimorphic systems, the nature of the comonomer can have a significant influence in the isodimorphic behavior. For instance, stereoregularity[23] and even-odd effects[23-26] are factors that can affect their behavior. Besides the combination of comonomers, other parameters that can affect the exclusion/inclusion balance, are thermal history[9, 19] and polymorphism.[27, 28]

The complex behavior of isodimorphic random copolymers is still far from being completely understood[9, 29] Hence, several types of research, in recent years, are devoted to this topic. Recent works have established[9, 29] that the isodimorphic character of random copolymers fits the following

criteria: (a) crystallization in all the compositions, despite their random distribution of counits; (b) a pseudo-eutectic behavior of the thermal properties (*e.g.*, melting temperature) as a function of the comonomer content; and (c) change of the unit cell parameters with the composition.

These criteria were mainly established under non-isothermal crystallization conditions. Isodimorphic copolymers have also been studied during isothermal crystallization. The isothermal test not only allows determining the crystallization kinetics, but also some essential parameters, such as the equilibrium melting temperatures, among others. Besides, the isothermal assay provides the information to apply exclusion/inclusion models, such as those developed by Flory,[30] Baur,[31] Sanchez-Eby[32], and Wendling-Suter.[33] In general, the crystallization kinetics of isodimorphic random copolymers depends on the composition, and also on the crystallization temperature (T_c). Consequently, the material crystallizes in the crystalline phase of one parent homopolymer or the other, according to the composition and T_c. Although under isothermal tests, we introduce an additional variable, *i.e.*, T_c, the obtained properties describe a pseudo-eutectic behavior as in non-isothermal tests.[8, 22]

The crystallization kinetics of isodimorphic random copolymers is expected to be slower and shifted to lower T_c in comparison with that of the parent components. The miscibility of the amorphous phases provokes a single composition dependent glass transition temperature (T_g) and a depression of the melting point of the crystallizable phase (as it will be surrounded by a molten solvent-like material).[8, 22] Even though several works have allowed obtaining general trends, the studies of isodimorphic copolymers sometimes have several shortcomings that have left open questions. Some of these shortcomings are: (a) The experimental limitations allow following the crystallization kinetics of only one of the components (*i.e.*, the one that crystallizes at higher crystallization temperatures). In some cases it is not possible to isolate the crystallization behavior

of the second component; (b) the crystallization kinetics of different random copolyesters has been reported without focusing in their isodimorphic response;[34] and (c) the quantification of the degree of comonomer inclusion is not precise, despite the used of different exclusion/inclusion models.

To study the above topics, we have selected poly (butylene succinate-*ran*-butylene adipate) (PBSA) isodimorphic random copolymers. These materials have a crystallization behavior that depends on the cooling rate employed. Additionally, their parent components have polymorphic behavior, originated by stretching (*i.e.*, PBS)[35, 36] or by temperature changes (*i.e.*, PBA).[19] Besides, these materials are also interesting from the degradation rate point of view and for their gas barrier properties. Both commercially available PBS homopolymer and PBSA copolymer have been used to prepare stretched films with excellent gas barrier properties for food packaging applications.[37] The biodegradation of these materials has been evaluated by their exposure to enzymes, compost, and microorganisms.[38-43] In general, better biodegradability[41] and gas barrier properties[37] have been found for the PBSA, evidencing the potential of the copolymerization as a strategy to tailor the final material properties. Tserki et al.[44] extent the degradation studies to different BS:BA compositions, and found that crystallinity regulates polymer degradation; therefore, those compositions with lower crystallinities showed faster degradation rates. On the other hand, the PBA biodegradability is related to its crystal structure, *i.e.*, polymorphism.[45-47] Despite the thermodynamic stability of the α-PBA phase, it exhibits a faster degradation rate than the β-PBA phase.[47] Thus, different strategies, such as blending,[46, 48, 49] and copolymerization,[28, 50] among others,[45, 47, 51, 52] have been used to control the polymorphic phase of the PBA and hence its degradation rate.

The non-isothermal crystallization of PBSA copolymers has been previously studied.[19] It shows a pseudo-eutectic behavior when their thermal properties (*i.e.*, crystallization and melting

temperatures, and their respective enthalpies) are plotted as a function of the composition. The pseudo-eutectic region was located at the intermediate compositions, BS:BA 50:50 and 40:60 (Tserki et al.[44] found that these compositions showed a higher degradation rate). These compositions crystallize with a strong influence on the cooling rate (*e.g.*, coincident crystallization and sequential cold-crystallization of the two types of crystalline phases were found depending on the cooling rate). Besides thermal analysis, *in-situ* WAXS/SAXS experiments revealed changes in the unit cell parameters and a pseudo-eutectic behavior of the lamellar thickness as a function of the composition.[19]

In this work, we study the influence of thermal history on crystallization by applying different thermal protocols. Three different thermal protocols were selected: non-isothermal, isothermal, and Successive Self-nucleation and Annealing (SSA) experiments. The isothermal crystallization and SSA fractionation of these copolymers have never been reported in the literature, as far as the authors are aware. The thermal and structural changes are studied by DSC and *in-situ* WAXS/SAXS experiments. The results of this characterization provide new information on the behavior of PBSA random copolymers under isothermal and SSA tests and on the influence of crystallization conditions on the exclusion/inclusion balance and polymorphism.

2. EXPERIMENTAL PART

2.1. Materials

The aliphatic random copolyesters of poly (butylene succinate-*ran*-butylene adipate) (PBSA) employed in this study were synthesized by a two-step melt polycondensation method. The details of the synthesis and chemical characterization can be found in our previous work.[19]

2.2. Differential Scanning Calorimetry

We employed a Perkin Elmer 8500 DSC equipped with an Intracooler III. The instrument operated with ultrapure nitrogen flow (20 mL/min) and was calibrated with indium and tin standards. Samples weighted *circa* 5 mg.

The following tests were performed, after erasing the thermal history by equilibrating the material at a temperature that is 30 °C above its melting temperature (T_m), to fully characterize the thermal and structural properties of the samples:

Isothermal tests

The isothermal tests followed the protocol of Lorenzo et al.[53] As a first step, we determined the minimum crystallization temperature, $T_{c,min}$. This crystallization temperature (T_c) is the minimum temperature that allows cooling the material (at 60 ºC/min) without causing any crystallization. Therefore, no melting endotherms should be found in the subsequent heating. The samples were cooled from the melt state until a selected T_c (*i.e.*, higher than the $T_{c,\,onset}$ determined by the non-isothermal test) at 60 °C/min. Then, they were immediately heated at 20 °C/min, recording their subsequent heating curve. If the recorded heating curve shows a finite melting endotherm (*i.e.*, this reflects that crystallization occurs during the previous cooling), then it is necessary to employ a higher T_c and repeat the process described above. But, if no endothermic peak (after the selected

T_c) is detected, the employed T_c would be the $T_{c,\,min}$. The $T_{c,min,}$ is employed as the starting T_c in the isothermal test. We applied this method to all the samples.

The isothermal crystallization experiments were then performed. The samples were cooled from the melt to a set T_c ($\geq T_{c,\,min}$), and held for a crystallization time (t_c) until completion of crystallization (a typical crystallization time of three times the peak value was employed to guarantee that the crystallization process at the selected T_c value was completed). After the crystallization has finished, the sample is heated from T_c at 20 ºC/min to determine the study the melting process after isothermal crystallization.

Self-nucleation (SN) and Successive Self-nucleation and Annealing (SSA)

SN experiments were performed before the SSA test. Keller et al.[54] developed self-nucleation procedures to study the formation of single crystals from solution, and Fillon et al. [55] adapted it to conventional DSC experiments in melt-crystallized samples. A recent work reviewed the SN procedure and its basics.[56]

By applying the SN test, we found the $T_{s,\,ideal}$ (*i.e.*, the temperature that causes the maximum SN without annealing) for all the samples. This temperature corresponds to the minimum T_s within *Domain II* of each material and is the starting point for SSA experiments. See the detailed procedure employed for SN in Section S1 and Scheme S1 of the Supporting Information.

Müller et al.[57-61] developed and recently reviewed the SSA technique. The technique was originally designed to study short chain branching distribution in ethylene/α-olefin copolymers but was subsequently extended to perform thermal fractionation to any material that contains defects that interrupt crystallizable sequence. The technique produces a distribution of lamellar thickness in the sample according to different crystallizable sequence lengths, which results in a distribution

of thermal fractions during the final DSC heating scan. The application of the SSA thermal program (*i.e.*, a careful combination of thermal ramps and holding steps) to a crystallizable polymer, promotes the formation of a distribution of crystal fractions characterized by different melting temperatures. The molecular fractionation that occurs during crystallization causes the above-mentioned thermal fractions. This experiment is performed in a conventional DSC, although its application on fast scanning calorimeters has also been reported .[57, 62]

Different works,[58-60] in the literature, report the detailed procedure to perform SSA, and its most critical parameters: the first self-nucleation temperature, the time spent at each T_s (*i.e.*, self-nucleation temperature), and the fractionation windows. The detailed procedure employed to perform the SSA tests can be found in Section S2: Table S1 and Scheme S2 of the Supporting Information.

In this work, we have used as a first T_s, the ideal self-nucleation temperature, $T_{s,ideal}$ for neat PBS (which is the component with the highest melting temperature of all the materials employed in this work), which corresponds to 114 ℃, the time spent at T_s was 5 minutes and the fractionation windows 5 ℃. We employ the same starting T_s for all the materials to apply the same thermal history and gain information on the relative differences in crystallizability.

2.3. Wide and Small-angle X-ray Scattering (WAXS and SAXS)

In-situ X-ray experiments were performed simultaneously to the application of a thermal protocol, either in isothermal conditions or according to the SSA test. Also, we performed the X-ray experiments on already prepared samples (*e.g.*, samples that underwent a previous thermal history). We performed these experiments in the European Synchrotron Radiation Facility (ESRF) and the ALBA synchrotron facilities, respectively.

WAXS/SAXS during the isothermal test

In-situ SAXS, and WAXS experiments were conducted at the beamline BM26-B at ESRF in Grenoble, France. We have placed each sample in a DSC pan and used a Linkam DSC600 hot-stage coupled to a liquid nitrogen cooling system. We programmed the hot-stage to perform cooling, holding, and heating steps (*i.e.*, isothermal test). At the same time, we took measurements of SAXS/WAXS patterns. For each sample, we selected at least three isothermal crystallization temperatures. SAXS/WAXS patterns were acquired in both isothermal and in the subsequent heating step. Pilatus detectors, 300k and 1M, were used to record the scattering pattern at wide and small angles. Table 1 shows the related technical information.

WAXS/SAXS during SSA test

WAXS and SAXS patterns were acquired simultaneously, during the heating scans applied to previously fractionated samples (inside DSC pans) placed in a Linkam THMS600 hot-stage coupled to a liquid nitrogen system. In the case of the intermediate compositions, we performed *in-situ* experiments by programming the whole SSA protocol in the hot-stage (*i.e.*, by reproducing the conditions used in the DSC experiments) and measuring the WAXS/SAXS patterns during the cooling, heatings and holding steps. We used ADSC Q315r and LX255-HS (Rayonix) detectors for the SAXS and WAXS measurements, respectively. Table 1 shows the related technical information.

Table 1. Main technical characteristic of the employed setups at the ESRF and ALBA synchrotron facilities.

Synchrotron	X-ray source (keV)	Sample-to-detector distance (mm)	Pixel size (μm^2)	Calibrant	Performed test
ESRF$_{SAXS}$	12 (λ=1.03 Å)	2946	172	Silver behenate	Non-isothermal and isothermal
ESRF$_{WAXS}$		274		Alumina poder	
ALBA$_{SAXS}$	12.4 (λ=1.0 Å)	6495	102	Silver behenate	SSA
ALBA$_{WAXS}$		132.6 (tilt angle of 21.2^0)	44	chromium (III) oxide	

The intensity profile analyzed as scattering intensity (I) vs. scattering vector, $q=4\pi sin\theta\lambda^{-1}$, where λ is the X-ray wavelength, and 2θ is the scattering angle. Table 1 shows the calibrants used to calibrate the scattering vector. The intensity has been corrected for background and sample absorption.

3. RESULTS AND DISCUSSIONS

We evaluated the influence of three different crystallization conditions in the exclusion/inclusion balance and polymorphism of PBSA random copolymers. Information was obtained by performing non-isothermal, isothermal, and Successive Self-nucleation and Annealing (SSA) experiments. Below, we discuss the influence of each test.

3.1. Non-isothermal experiments

In our previous work,[19] we evaluated PBSA random copolymers under non-isothermal conditions with DSC and X-ray experiments. We have identified the isodimorphism of the PBSA copolymers, following the established criteria, which have been applied to other random copolymers.[2, 3, 13, 21, 33-38]

Besides the isodimorphism of PBSA copolymers, we also found a strong influence of the thermal history on the behavior of intermediate compositions, *i.e.*, those within the pseudo-eutectic region. Figure S1 (see Supporting Information, SI) shows the cooling and subsequent heating DSC scans for all the samples. Below, we summarize the most relevant results. For further details, see reference.[19]

The non-isothermal experiments revealed that the copolymer samples can crystallize in their entire composition range, and their behavior can be divided into three regions, depending on the composition: *PBS-rich* (PBS, 80:20, and 60:40 PBSA), *PBA-rich* (PBA, 20:80 PBSA), and the *pseudo-eutectic* region (50:50 and 40:60 PBSA).

The crystallization and melting temperature (as well as the crystallinity degree) decrease as the comonomer content (BA or BS, respectively) increases in the *comonomer-rich regions* (PBS-rich and PBA-rich). Such decreases reach its minimum in the transition or *pseudo-eutectic region*, in this case, at intermediate compositions. The described regions are characterized by changes in the *d*-spacing, calculated from the WAXS patterns, as the comonomer content increases. The largest *d*-spacing changes were found in the *pseudo-eutectic* region. This region is characterized by the possible crystallization of both PBA-rich and PBS-rich phases, but they show a crystallization behavior highly dependent on the cooling rates applied. For more details, see reference.[19]

The strong dependence of the crystallization in the *pseudo-eutectic* region on the cooling rates, opens the following question: How do the crystallization conditions affect the comonomer excluded/included fraction in PBSA isodimorphic copolymers? To answer this question, we have performed isothermal crystallization and SSA fractionation experiments by DSC and *in-situ* X-ray diffraction.

3.2. Isothermal experiments

Isothermal crystallization experiments are in principle closer to thermodynamic equilibrium, as compared with the non-isothermal tests. However, kinetic factors also play a crucial role in the isothermal crystallization of polymeric materials. As a consequence, the resulting isothermally crystallized copolymers could have a different balance of exclusion/inclusion of comonomeric units in comparison to non-isothermally crystallized samples.

During the isothermal crystallization test, the crystallization kinetics is dominated either by the PBS-rich or the PBA-rich phase. Also, the crystallization temperature (T_c) strongly affects the crystallization kinetics. For instance, in the pseudo-eutectic composition of 40:60 PBSA, when a low T_c is employed, the crystallization is dominated by the PBA-rich phase, but with a small influence of the PBS-rich phase. In contrast, at high T_c, the crystallization is driven by the PBS-rich phase. For this 40:60 PBSA composition, the particular crystallization and melting behaviors evidence the dominant phase (*i.e.*, PBS-rich vs. PBA-rich) (see Figures S2 to S4). For all the other compositions, only one of the two phases present dominates the crystallization behavior at all T_c values. This behavior is explained in detail below.

3.2.1. Experimental overall half-crystallization rates and melting behavior

Figure 1a shows the inverse of the overall half-crystallization times ($1/\tau_{50\%}$) as a function of T_c for the random copolymers. The values of $1/\tau_{50\%}$ are an experimental measure of the overall crystallization rate (a quantity that includes both primary nucleation and growth). The isothermal DSC curves for all materials can be found in Figure S2 of the SI. The experimental $1/\tau_{50\%}$ values have been fitted to the Lauritzen and Hoffman theory[63, 64] applied to DSC experiments[65-69] (see Section S5 and Figure S5 of the SI).

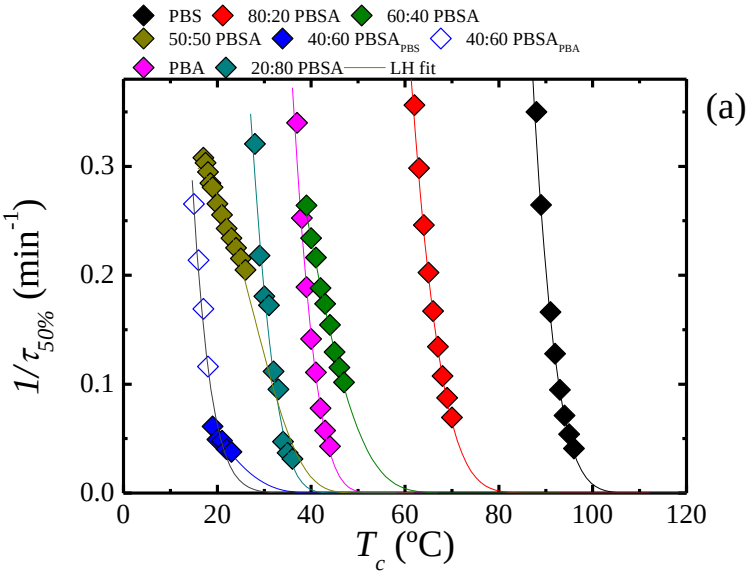

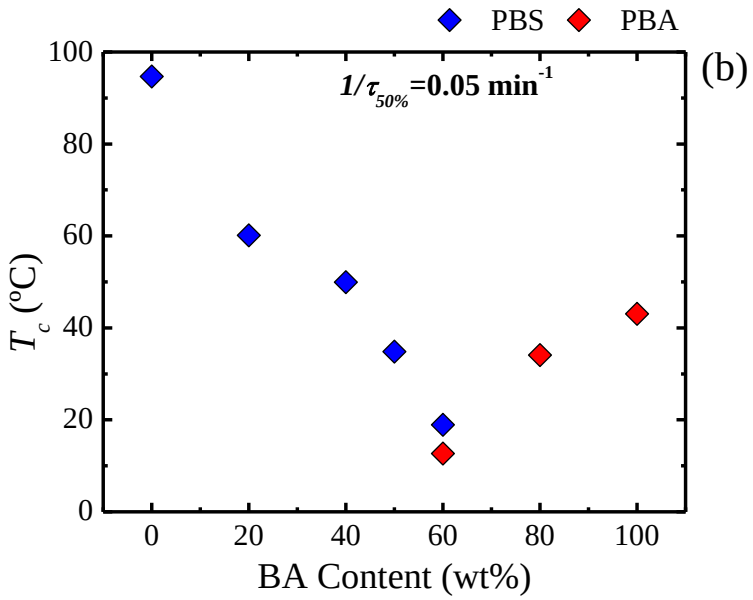

Figure 1. (a) Overall crystallization rate (expressed as the inverse of the half-crystallization time) as a function of T_c for the indicated systems and (b) T_c values as a function of BA content at a constant value of $1/\tau_{50\%}$=0.05 min^{-1}.

In Figure 1a, we observe that PBS-rich compositions (*i.e.*, PBS, 80:20, and 60:40 PBSA) crystallize at higher T_c (right-hand side of the plot). However, the available T_c range, as well as the $1/\tau_{50\%}$ values, show a decrease as BA content increases. This implies a relative reduction in the PBS-rich phase crystallization kinetics which is probably caused by the partial BA counit exclusion from the PBS-like crystals, together with a plasticization or "solvent-effect" caused by the molten BA-rich segments. These molten segments increase the chain mobility of the PBS and reduce its crystallization temperature. A similar trend is observed at intermediate T_c range, where the PBA-rich compositions (*i.e.*, PBA and 20:80 PBSA) crystallize. In this case, the achievable T_c, as well as $1/\tau_{50\%}$ values, decrease with the increase in BS content. In an analogous way, this could

be attributed to the BS counit exclusion from the PBA-like crystals and a "solvent-effect" of the molten BS-rich sequences.

At the pseudo-eutectic region (*i.e.*, 50:50 and 40:60 PBSA), the PBSA copolymers crystallize at the lowest T_c values (maximum supercooling), see Figure 1a. Also, the slope of the curves changes in comparison with that of the neat components. These changes indicate a different balance of factors (*i.e.*, exclusion/inclusion balance vs. "solvent effect") at the intermediate or pseudo-eutectic compositions, in comparison with the PBS-rich and PBA-rich regions. Such behavior is in line with the larger changes observed in *d*-spacings to be discussed below in Section 3.4.2.

The isothermal crystallization kinetics of the 50:50 PBSA sample in Figure 1a is dominated by the generation of exclusive PBS-rich phase crystals in all the T_c range used. We previously found[19] that when this sample is crystallized by slow cooling from the melt (5 ºC/min), both PBS-rich and PBA-rich phases could crystallize. Such coincident crystallization occurs only partially at a cooling rate of 20 ºC/min, since the subsequent heating shows a cold-crystallization related to the PBA component (see Figure S1 and reference 19 for more details). In the present case, when the sample is crystallized isothermally, PBS-rich phase spherulites are formed and crystallize to saturation. They prevent any PBA-rich phase crystallization, most probably by a confinement effect (as the PBA-rich phase would have to crystallize within the interlamellar spaces of the PBS-rich spherulites).[19]

In the special case of the 40:60 PBSA sample, both PBS-rich and PBA-rich phases can crystallize depending on the T_c value. At T_c<19 ^{o}C, the PBA-rich crystal phase is formed together with the PBS-rich crystal phase (as demonstrated by WAXS below, see Figure 3). On the other hand, at T_c>19 ^{o}C, only PBS-rich crystals are formed.

Figure 1a, shows that the overall crystallization rate at T_c>19 ºC, corresponding to the PBS-rich phase of the 40:60 PBSA copolymer, is much lower than that at T_c<19 ºC. At these low crystallization temperatures, both crystalline phases are formed. It is expected that the PBS-rich phase crystals form first, at shorter times, and could nucleate the PBA-rich phase crystals. This nucleation effect together with the lower crystallization temperatures possibly promote a combined faster crystallization kinetics of both phases. The isothermal DSC curves corresponding to this 40:60 PBSA sample are shown in Figure S2 of the SI. The DSC isotherm always shows a unimodal character regardless of whether one or both phases can crystallize, but the sudden change in crystallization rate at 19 ºC is easily seen. In the case of high T_c, the PBS-rich phase hinders any crystallization of the PBA-rich phase in the 40:60 PBSA sample (also demonstrated by WAXS in Figure 3). As a result, the high amount of molten PBA-rich chains, together with counit exclusion, causes a decrease in overall crystallization rate (Figure 1a).

Figure 1b shows a plot of the T_c values required to obtain a constant overall crystallization rate in all the materials, given by $1/\tau_{50\%}$= 0.05 min^{-1}. The plot shows a pseudo-eutectic trend similar to that observed when several calorimetric quantities are plotted as a function of composition. [8, 22]

Due to the different exclusion/inclusion balance related to the crystallization conditions, the limits of the pseudo-eutectic region change. In our previous study of the non-isothermal crystallization of these samples,[19] we showed that both phases could crystallize for both 50:50 and 40:60 PBSA compositions when the samples were cooled at 5 ºC/min. In contrast, the isothermal experiments show single-phase crystallization for the 50:50 composition and the crystallization of the two PBS-rich and PBA-rich phases only at low T_c in the 40:60 PBSA sample.

As explained in the experimental part, DSC heating scans after isothermal crystallizations were performed to determine the melting points of the generated crystals. Then, using the

Hoffman-Weeks[70] approach, the equilibrium melting points of all samples were calculated. Details and corresponding data can be found in Section S6 of the SI.

The obtained equilibrium melting point values (T_{m0}) are plotted as a function of composition in Figure 2a. The T_{m0} values for the parent components are in line with the range reported in the literature for PBS,[71-73] *i.e.*, 127.5 to 146.5 °C, and PBA,[74] *i.e.*, 58 to 73 °C. The presence of a eutectic point located at a composition of 60% BA content (40:60 PBSA sample) is evident. The two data points at the eutectic composition correspond to the PBS-rich and PBA-rich phase crystals. In this case we use the term eutectic (instead of pseudo-eutectic, normally employed to indicate that the measurements were not performed at equilibrium), as Figure 2a represents equilibrium conditions (obtained by the Hoffman-Weeks extrapolation).

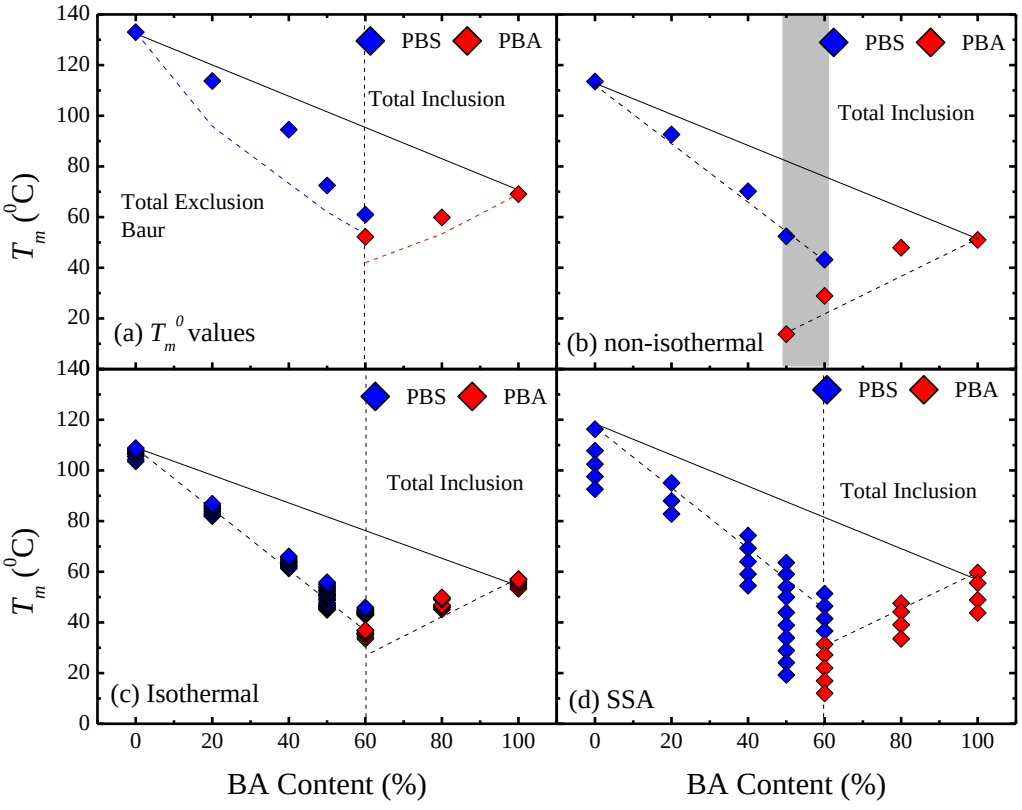

Figure 2. T_m values versus BA content for (a) T_{m0} (equilibrium melting temperature) values obtained by Hoffman-Weeks extrapolation after isothermal crystallization; (b) Experimentally determined peak melting temperatures after non-isothermal crystallization at 5 ºC/min, data taken from our previous work[19]; (c) Experimentally determined peak melting temperatures after isothermal crystallization (several data points are plotted at each composition and they correspond to different isothermal crystallization temperatures) and (d) Experimentally determined peak melting temperatures obtained during the final DSC heating scan after SSA tests (several data points are plotted at each composition and they correspond to the melting points of the different thermal fractions obtained). The dotted lines in (a) represent the total comonomer exclusion case given by the Baur model. Note that in all the figures the total comonomer inclusion case is represented with a solid line. The dashed lines in (b) are arbitrary fits to the experimental data, which were also drawn in (c) and (d) for comparison purposes. The vertical dashed lines in (a), (c) and (d) represent the position of the pseudo-eutectic point, and the shadowed region in (b) represent the pseudo-eutectic region.

Regarding the balance between comonomer inclusion/exclusion, we show in Figure 2a the two extreme theoretical cases. Total inclusion is represented by a simple mixing law, which has been observed for isomorphic random copolymers,[14] where both comonomers can crystallize in a single unit cell type in the entire composition range. On the other extreme, total comonomer exclusion has been represented in Figure 2a by applying the Baur model (see Section S7 of the SI) for a full description of the model and how the calculation was performed). The predictions of the Baur model are represented in Figure 2a with dotted lines. The data points for the PBSA copolymers lay in between the two extreme cases. Nevertheless, it can be seen that the data points are closer

to the exclusion model than to total inclusion. Therefore, at least under thermodynamic conditions, it is predicted that these copolymers have more comonomer exclusion and that comonomer inclusion is limited and composition dependent.

Figure 2b shows the experimental trends observed by melting the samples after non-isothermal crystallization (*i.e.*, cooling at 5 ºC/min), while Figure 2c shows a similar type of plot for isothermally crystallized samples. The trends are very similar and they also display a clear pseudo-eutectic behavior. The dashed lines in Figure 2b represent an arbitrary fit to the data. The same dashed lines were drawn in Figure 2c (somewhat shortened to fit the data points) for comparison purposes and the fit of the data is very good. From the trends in melting point values, no large qualitative differences are observed between isothermally and non-isothermally crystallized samples, except for the fact that in the non-isothermal case, two crystalline phases are produced both in the 50:50 and 40:60 sample, but in the isothermal case, only the 40:60 sample was able to develop double-crystallinity at low T_c values (see vertical dashed lines and shadowed region in Figure 2).

The trends in melting points (*i.e.*, pseudo-eutectic behavior) were also found in lamellar thickness (Figure S8), and percentage of crystallinity (X_c) (Figure S9 and S10) (see Section S8 of the SI for more details). The X_c should be the highest in the case of total inclusion and the lowest for total exclusion. In the latter, we expect that the X_c values drop to zero at a specific composition. In contrast, in the total inclusion (*e.g.*, isomorphic case[10-14]), the X_c values keep a high level,[13, 75] or increases ("uniform inclusion"),[27] as a function of the composition. We found a decrease of the X_c values for both PBS and PBA-rich composition. Such a decrease describes a pseudo-eutectic behavior independently of the crystallization condition. But, the most significant changes are

related to the SSA test, suggesting a different counit inclusion behavior, caused by the change in PBA crystal polymorphism (*i.e.*, α vs. β-PBA phases).

To get more insights on the possible comonomer inclusion/exclusion balance differences between the samples, WAXS experiments were performed to probe crystal dimensions.

3.2.2. Isothermal WAXS/SAXS experiments

In-situ WAXS/SAXS experiments were conducted at identical conditions to those performed by isothermal DSC tests. Figure 3 shows the WAXS patterns for all the materials at selected low (Figure 3a) and high (Figure 3b) T_c values (*i.e.*, each sample at its own T_c indicated in the plot). Table S4 (SI) shows the long periods and lamellar thickness calculated from the SAXS patterns.

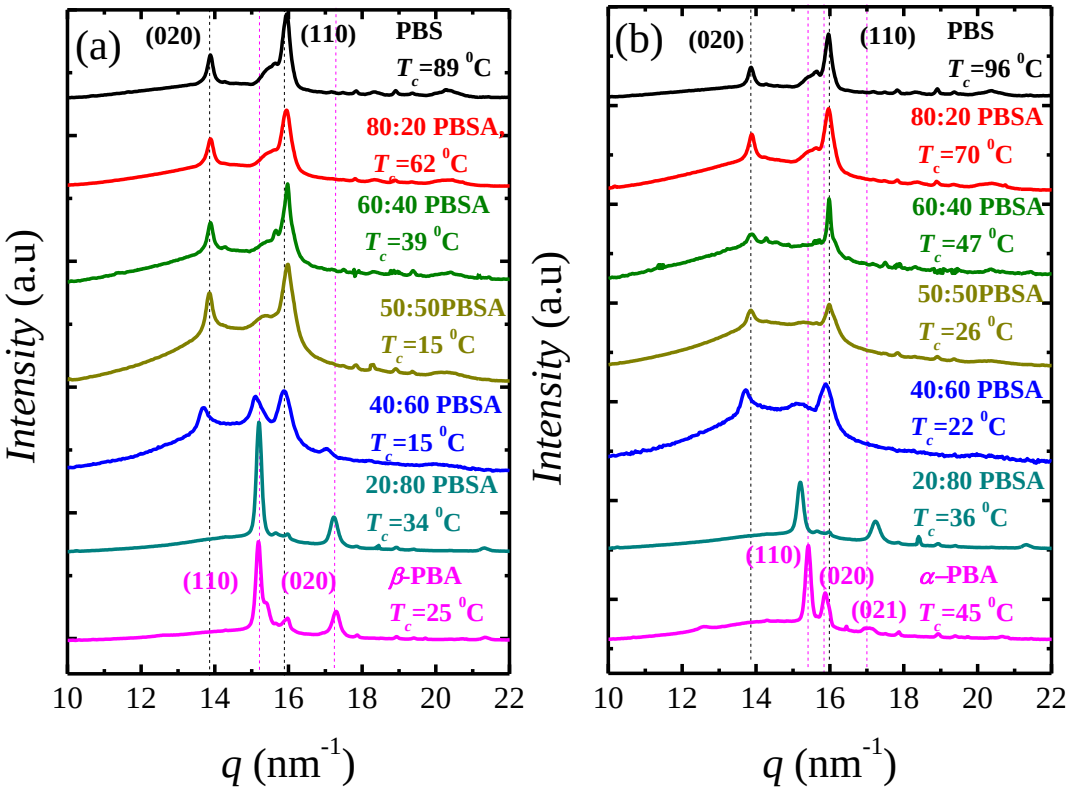

Figure 3. WAXS patterns for all the investigated materials at the indicated (a) low and (b) high T_c values. Note that the WAXS pattern of the 40:60 PBSA sample strongly depends on the T_c used. Dotted lines are used to indicate the main reflections of the homopolymers.

PBS crystallization

Figure 3a shows that the PBS-rich samples (including the 50:50 PBSA) have WAXS patterns that resemble that of neat PBS. Therefore, the main reflections appear at *d*-spacings (calculated from the main *q* values with Bragg's Law) of 0.452 (13.9 nm^{-1}) and 0.395 nm (15.9 nm^{-1}), corresponding to the *(020)* and *(110)* PBS planes, respectively. Additionally, medium-intense reflections are found at *d*-spacings of 0.403 (15.6 nm^{-1}) and 0.310 nm (20.3 nm^{-1}) and correspond to the *(021)* and *(111)* planes.[34, 38, 44, 76, 77] We assign these different planes to the monoclinic unit cell of α-PBS,[34, 36, 38, 77] with unit cell parameters of a=0.532, b=0.9057, c=1.090 nm, and β=123.87[0.36] The PBS also shows a β-form (not observed in this work) that can be obtained by stretching[78]. The β-PBS also belongs to the monoclinic system, with a=0.584 nm, b=0.832 nm, c=1.186 nm, and β=131.6[0.36] In the α-PBS (obtained under normal conditions[78]) the molecular conformation is $TGT\bar{G}T$ (*i.e.*, T=trans, G=gauche, and $\bar{G}$=minus gauche). In contrast, the β-PBS is a planar *zigzag* (all-trans or *TTTTT*).[35, 36] The α-β transition occurred reversibly upon loading and unloading.[78] In this work, we always obtained the α-PBS crystal form.

The same reflections are observed for PBS and PBS-rich samples as T_c increases (see Figure 3b), but they shift to lower *q* values (therefore higher *d*-spacings (see Figures 7a and b and their discussion below)) with the increase of BA content.

PBA crystallization: From α to β-PBA crystal phase

The PBA-rich WAXS diffractograms resemble that of neat PBA. PBA is a polymorphic material that shows a temperature-dependent crystallization behavior.[28] It can crystallize in the α or β-phase, depending on the T_c value employed. Figure 3 shows that all the PBA-rich copolymers crystallize in the β-PBA phase. For comparison purposes, in Figure 3a, we show the β-PBA phase, in the parent PBA homopolymer, induced by its crystallization at 25 °C. We found the β-PBA main reflections at *d*-spacings of 0.414 (15.2 nm^{-1}) and 0.363 nm (17.3 nm^{-1}) corresponding to the *(110)* and *(020)* planes, respectively. This polymorphic phase of PBA crystallizes in an orthorhombic unit cell with unit cell parameters of a=0.506 nm, b=0.735 nm, and c=1.467 nm.[79-83] By testing the temperature-dependent PBA crystallization, we found that it forms only β-phase at 25 °C; α+β-phase at 30 °C, and only α-phase at 35, 38 and 45 °C (see Figure S11), corroborating previously reported results in the literature.[74, 84]

The PBA-rich copolymers crystallize in the β-PBA crystal form, and their *d*-spacings increase as the BS content increases (see Figure 7a, to be discussed in detail below). However, the *d*-spacings remain almost unchanged as T_c increases. The presence of the β-PBA crystal phase in the copolymers is possibly related to the BS comonomer unit inclusion in the PBA crystalline unit cells. Liang et al. found in PBA-*ran*-PHA copolymers that the HA inclusion stabilizes the β-PBA form, even at T_c as high as 35 °C.[28] They concluded that, due to the lattice matching, the HA units are better tolerated in the β-PBA crystalline unit cells than in the α-PBA phase.[28] On the other hand, it is worth noting that in PBS/PBA blends, the presence of PBS chains favors the crystallization of the PBA in its α-phase.[76]

As expected, at high T_c, *i.e.*, 45 °C, neat PBA crystallizes in its α-phase (see Figure 3b). We found the main characteristics reflection of the α-PBA at *d*-spacing of 0.411 (15.3 nm^{-1}) and 0.398

(15.8 nm^{-1}), and a medium intense reflection at 0.370 nm (17.0 nm^{-1}), corresponding to the planes *(110)*, *(020)* and *(021)*, respectively.[34, 38, 44, 74, 76, 85] The α-PBA crystalline phase is characterized by a monoclinic unit cell with unit cell parameters of a=0.670 nm, b=0.800 nm, c=1.420 nm, and γ=45.5[0.38] Interestingly, the BA-rich copolymers crystallize in the β-PBA phase even at high T_c.

Crystallization of the 40:60 PBSA: Pseudo-eutectic composition

The WAXS patterns of the 40:60 PBSA reflect that its crystalline structure depends on T_c, as deduced from the isothermal DSC results. At low T_c values (*i.e.*, T_c=15 ℃), the WAXS patterns of the 40:60 PBSA copolymer show the main crystalline reflections of both homopolymers (PBS and β-PBA), see Figure 3a. In contrast, at high T_c (*i.e.*, T_c>15 ℃), the WAXS patterns of the 40:60 PBSA show crystalline reflections that only correspond to the PBS-rich crystal phase (see Figure 3b, with T_c=22 ℃). The PBS-rich phase crystallization dominates the kinetics (*i.e.*, at high T_c) due to their faster crystallization at higher temperatures, as compared to the PBA-rich phase. In this particular case (at T_c>15 ℃), the crystallization of the PBS-rich phase hinders the crystallization of the PBA-rich chain segments.

3.3. Successive Self-nucleation and Annealing (SSA)

SSA is a thermal fractionation technique that can be performed in a conventional DSC, or in a chip calorimeter (*i.e.*, like the Flash-DSC). Its design produces a distribution of lamellar crystals or thermal fractions. The SSA technique is very sensitive to the presence of defects that interrupt the crystallizable chain sequence length.[58] Therefore, we used it to detect differences among the random copolymers.

3.3.1. DSC Analysis of the SSA experiments

The comonomer exclusion from the crystalline lattice, in random copolymers, leads to an interruption of the crystallizable segments. As a result, we obtain an SSA profile of all the samples, which allows gaining further information on the thermal behavior of isodimorphic copolymers.

As neat PBS is the material with the highest melting point amongst all samples employed in this work, it was chosen to perform self-nucleation (SN) experiments. From the SN results (see Section S10 in the SI), we were able to calculate the ideal self-nucleation temperature ($T_{s,ideal}$), which is the temperature needed to start the SSA protocol. This $T_{s,ideal}$ is the self-nucleation temperature that produces the maximum number of self-nuclei without causing any annealing, or the minimum temperature within *Domain II* or self-nucleation *Domain*.[55, 60] The ideal SN temperature for PBS is 114 ºC (see Figure S12 and Table S5). This $T_{s,ideal}$ was employed as the first T_s value for the SSA fractionation of PBS. In order to compare the thermal fractionation results, we applied the same SSA protocol to all the samples with identical conditions: $T_{s,ideal}$ =114 ºC, fractionation window of 5 ºC and holding time at each T_s of 5 min (see details in Section S10 of the SI).

Figure 4 shows the final DSC heating scan after the SSA protocol for all the samples. Each sample displays a series of melting peaks or thermal fractions generated by the SSA protocol. As $T_{s,ideal}$ does not cause any annealing (*i.e.*, it only produces self-nucleation, see ref.60), in the case of the neat PBS sample, fraction 1 (highest temperature melting peak, labeled 1 in Figure 4) is produced by the annealing caused during the 5 minutes at $T_{s,1}$ (dotted vertical lines in Figure 4 indicate the T_s values). Fraction 2 by the annealing caused at $T_{s,2}$ and so on. PBS displays 5 thermal fractions or distinct melting peaks. The final DSC scans in Figure 4 represent a deconvolution of the standard DSC scan into elemental thermal fractions, hence the distribution of melting points is

clearly appreciated. At the same time, remembering that each T_m value has associated a lamellar thickness, the final DSC scan after SSA also represents a distribution of lamellar thickness in the sample.[60]

In the case of neat homopolymer samples like PBS and PBA, the fractionation is produced by molecular segregation during crystallization driven by differences in the molecular weights of the chains that are present, as the polymers are polydisperse. However, in the copolymers, the exclusion of comonomeric units is also present and it significantly improves the quality of the fractionation and also changes the distribution of the fractions, as judged by the areas under each fraction.

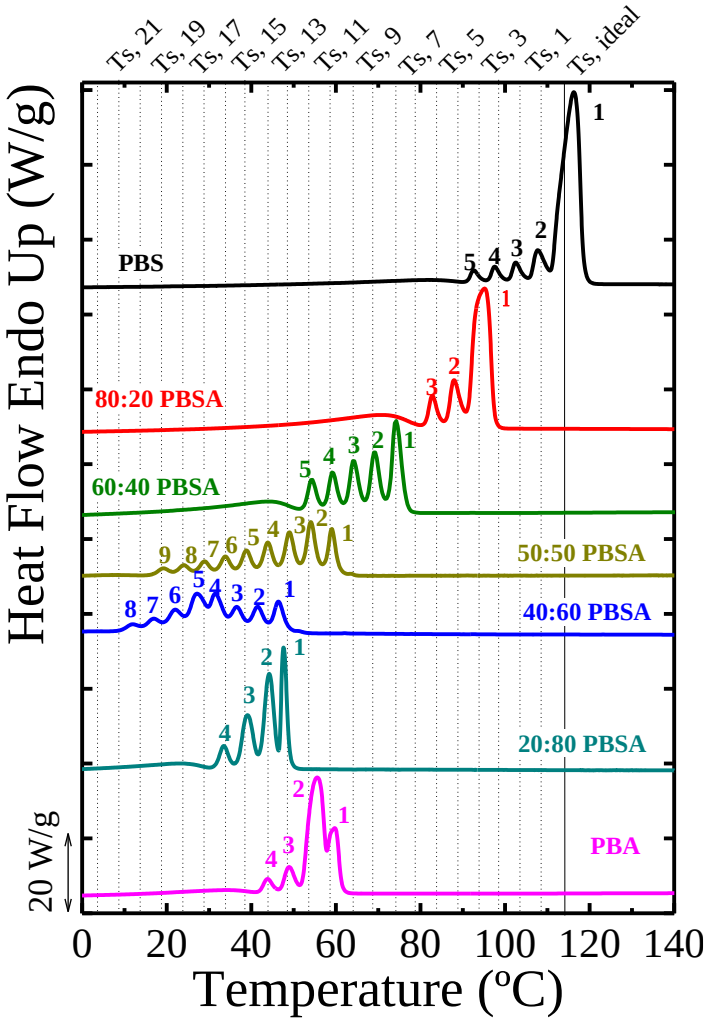

Figure 4. Final DSC heating scans for SSA fractionated samples. The solid vertical line represents the $T_{s,\ ideal,}$ and the dotted vertical lines represent the different T_s values employed. In the top part, the T_s are numbered as a guide. Each melting peak corresponds to a thermal fraction that are numbered starting from the highest temperature peak for each material.

To analyze the PBS-rich compositions (80:20, 60:40, and 50:50), we can compare the highest temperature melting peaks (fractions labeled 1 in Figure 4) and observe that they decrease as the BA content increases (see Figure 2d). A broad but unimodal (*i.e.*, produced by only one crystalline phase) distribution of melting fractions is observed in these compositions, indicating the absence of PBA crystals. Changes in the neat PBA and PBA-rich compositions (20:80) also indicate a decrease, as expected of the melting point of the fractions upon BS incorporation (see Figure 2d).

The trends shown in Figure 4 (*i.e.*, decreasing of the highest melting peak with comonomer content) describe a pseudo-eutectic behavior, as represented in Figure 2d above. Although the SSA is a different crystallization condition, it also gives rise to a pseudo-eutectic behavior. In this case, the pseudo-eutectic region corresponds only to the 40:60 composition (as in isothermal experiments at low T_c), instead of including the 50:50 and 40:60 compositions, as in the non-isothermal test (see Figure 2).

In the 40:60 composition, we found a bimodal distribution of melting points by SSA, indicating the presence of both PBA-rich and PBS-rich phase crystals. The fractions with lower T_m values (*i.e.*, fractions labeled 4-8 for the 40:60 PBSA curve in Figure 4) correspond to the PBA-rich crystals, and the ones with the highest T_m (*i.e.*, fractions labeled 1-3 for the 40:60 PBSA curve in Figure 4) correspond to the PBS-rich crystals. This result corroborates the concomitant crystallization of the two types of crystals found for this 40:60 composition in non-isothermal and

isothermal conditions (at low T_c values). On the other hand, for the composition 50:50, all melting peaks corresponding to 9 thermal fractions in Figure 4 are due to the melting of PBS-rich phase crystals (as proven by WAXS experiments in Figure 5).

To further understand the response of the materials under SSA experiments, we analyzed the structural behavior with X-ray experiments.

3.3.2. X-ray analysis of the SSA fractionated samples

We applied the SSA protocol, without the final heating, to all the samples. Then, at room temperature, we acquired WAXS/SAXS patterns. Figures 5 and S13 show the WAXS and SAXS patterns, respectively. Additionally, we performed the final heating *in-situ* at the synchrotron (see Figure S14).

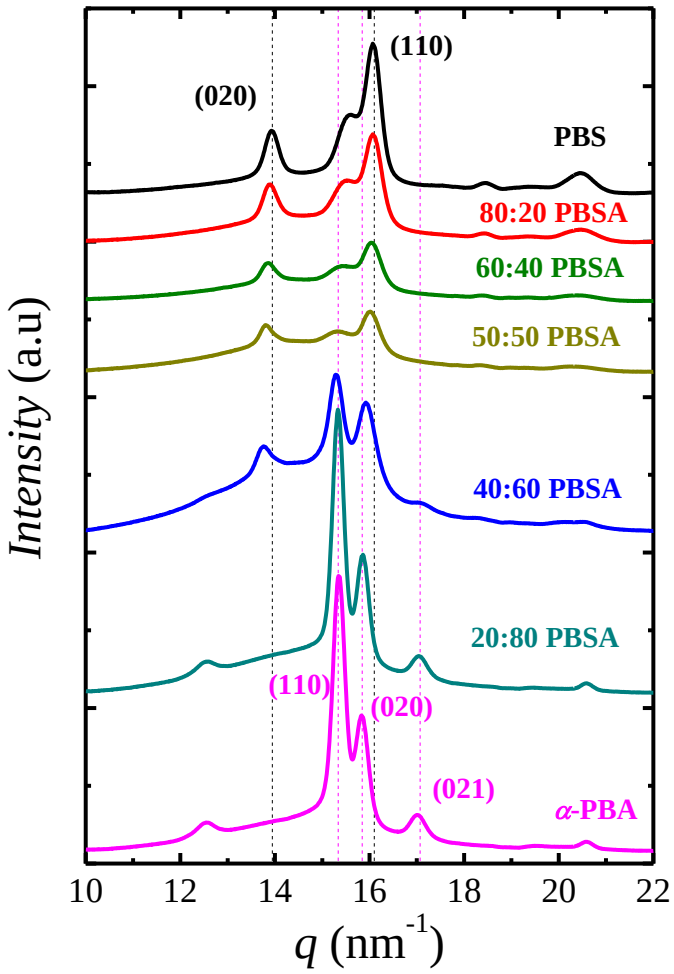

Figure 5. WAXS patterns for all the SSA fractionated samples before the final heating scan measured at room temperature, except for the 50:50 and 40:60 PBSA (*i.e.*, the WAXS pattern for these samples were taken at -40 °C in view of their lower melting point onset, see Figure 4). The dotted lines indicates the position of the main crystalline planes of the homopolymers.

Figure 5 shows presence of two crystalline phases, corresponding to PBS and PBA-like crystals, depending on the composition. At the top of Figure 5, we observed the WAXS patterns for PBS or PBS-rich crystals (*i.e.*, PBS, 80:20, 60:40, and 50:50 compositions), and at the bottom,

the ones for PBA and PBA-rich crystals (*i.e.*, PBA and 20:80 composition). The 40:60 PBSA sample contains both crystal types, as already anticipated in Figure 4.

The SSA protocol generates a significant change, in the PBA-rich compositions, since both neat PBA and the PBA-rich copolymers now crystallize in the α-PBA phase instead of the β-PBA phase (see Figure 3). We recall that the β-PBA form instead dominates the crystallization for non-isothermal and isothermal experiments.

As in the non-isothermal and isothermal tests, the 40:60 composition shows a WAXS pattern, after the applied thermal protocol, with both PBS-rich crystals and, in this case, α-PBA-rich crystals. Section S11 shows the melting behavior analysis of the 40:60 PBSA. The change from α to the β-PBA phase opens the question of why the SSA protocol promotes the formation of the α-PBA phase? Below we analyze the WAXS experiments in detail to try to understand the generation of the crystalline phases during SSA.

Understanding the successive self-nucleation and annealing process in the BA-rich compositions: the 40:60 PBSA composition as a case study

Figure 6 shows the evolution of the crystalline polymorphic structures (*i.e.*, α- and β-PBA phases) during the SSA protocol.

Figure 6b shows WAXS patterns of the 40:60 sample taken during the holding step at the indicated T_s values (*i.e.*, during the 5 minutes at T_s) (see the indicated T_s in Figure 6a). Figure 6c shows the WAXS patterns taken during the holding steps at -40 °C (*i.e.*, 1 minute at -40 °C, after cooling from T_s at 20 °C/min). We indicate the number of SSA steps at the bottom of Figure 6a and in brackets in Figure 6c. We use them in the plot shown in Figure 6d.

Figure 6d shows the evolution of the WAXS peak intensity and *d*-spacing of the *β-(110)PBA* or *α-(110)PBA* plane (see Figure 6c) during the SSA process (*i.e.*, number of steps). We have selected this plane for clarity; for details of the other planes see Figure S15c in the SI.

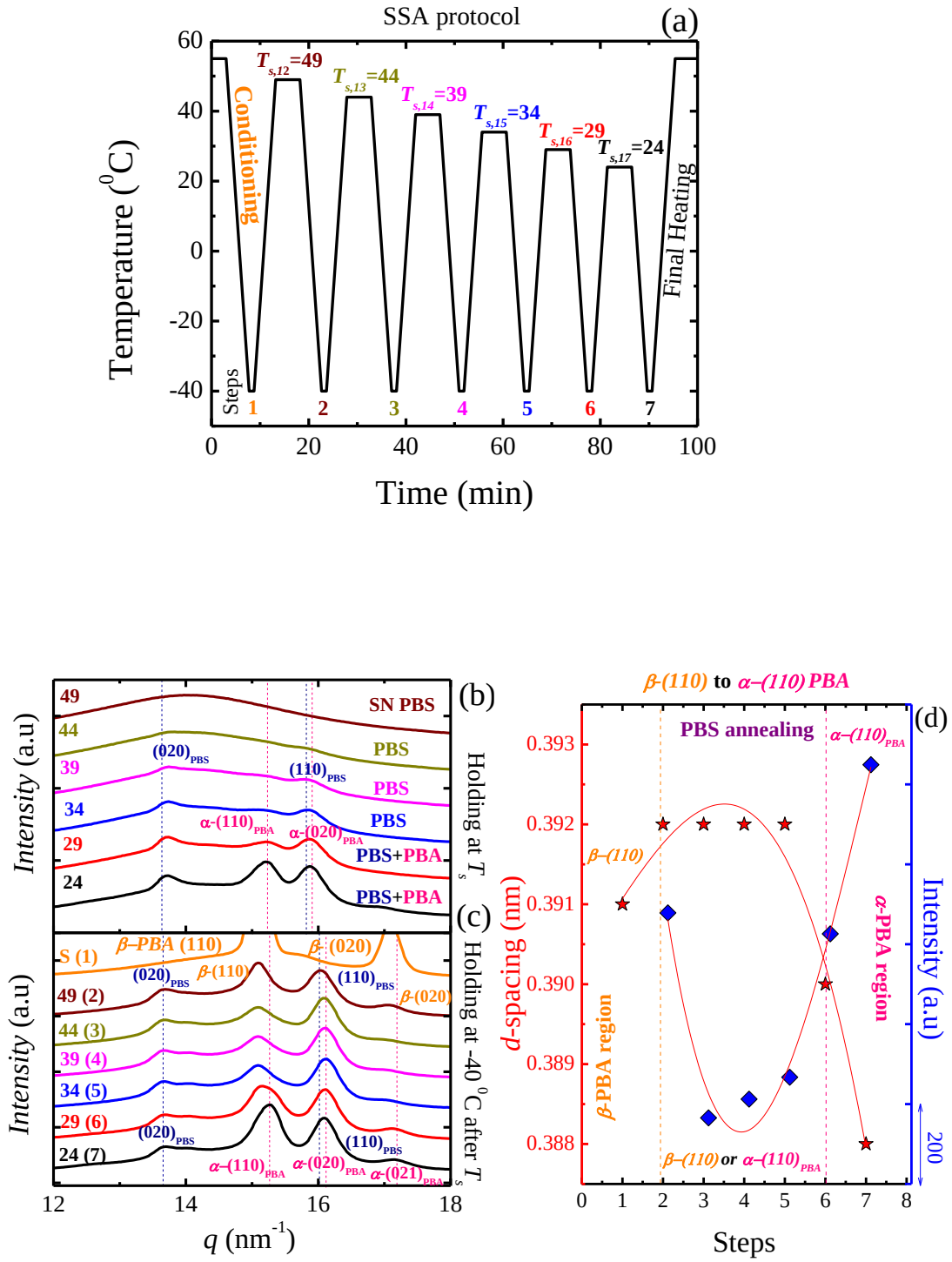

Figure 6. Influence of the number of SSA steps performed to the 40:60 PBSA sample: (a) Applied thermal protocol. We indicate the T_s value following the same notation as Figure 4 (see T_s indicated at the top), and SSA step number (inside the figure at the bottom). WAXS patterns taken at (b) the indicated T_s values (top) and (c) -40 ºC, after cooling the sample from the indicated T_s values (bottom). The numbers at the bottom of Figure 6a and in brackets in Figure 6c represent the SSA step number. (d) Evolution of the intensities of WAXS reflections corresponding to (110) PBA plane. Note that this plane can belong to the β or α-PBA phase depending on the Step. Figure 6d is divided into three regions, depending on the observed changes in the different phases in Figures 6b and c.

Based on Figure 6, the evolution of the crystalline structure during the SSA fractionation protocol can be explained in three regions, as follows:

Region a: Standard State

According to the SSA protocol (see Figure 6a and Scheme S2 in the SI) the sample is first melted to erase all its thermal history. Then it is cooled from the melt at 20 ºC/min down to -40 ºC. During this cooling, the sample achieves a standard thermal history (that given by the controlled cooling in the DSC at 20 ºC/min). In this initial state, before applying the SSA protocol, the PBA-rich phase crystals in the 40:60 PBSA are in their *β*-PBA phase (see Step 1 in Figure 6c and the indicated domain in Figure 6d). The sample at this stage (before the SSA protocol is applied) has the same degree of comonomer inclusion/exclusion balance as in non-isothermal experiments.

Region b: Self-nucleation and annealing of the PBS-rich phase: Coexistence of PBS-rich and PBA-rich phase crystals

The highest T_s applied to the sample (*i.e.*, 49 ℃) melts the *β*-PBA crystals (see the WAXS curve in Figure 6b) and self-nucleates the PBS phase within the copolymer (40:60 PBSA) before the sample is cooled to -40 ºC. The self-nucleation of the PBS-rich phase favors its crystallization during cooling (*i.e.*, from T_s to -40 ℃). Even though the PBS-rich phase crystallizes first (at higher temperatures), the PBA-rich phase also crystallizes during cooling from the melt. Consequently, at -40 ℃, both phases are present and are shown in Figure 6c (*e.g.*, see curve at T_s=49 ℃).

At lower T_s values (*i.e.*, 44 to 34 ℃, see steps 3 to 5, indicated in Figure 6d as PBS annealing), the WAXS patterns at these holding steps evidence the annealing of the PBS-rich phase. Even though the *β*-PBA continues crystallizing (see the peaks corresponding to *β-(110)* and *β-(020)* in Figure 6c), the intensity of the peaks (in particular the *β*-(110)) decreases, while their *d*-spacing does not change (see Figure 6d and Figures S15a and b), indicating a saturation of the BS inclusion in these steps (3 to 5). Therefore, we denoted this region as the PBS annealing zone in Figure 6d.

Region c: Annealing of the PBA-rich phase crystals

At the lowest T_s values (*i.e.*, 29 to 24 ℃, see steps 6 and 7), the PBA-rich crystals start to anneal, as can be seen in the holding steps at T_s (see vertical dashed lines indicating the $\alpha\text{-}(110)_{PBA}$ and $\alpha\text{-}(020)_{PBA}$ peaks in Figure 6b). The annealing process at such low T_s would favor the crystal matching sequence of the BA with itself instead of with BS segments. Then, with enough BA sequences, a transformation from *β* to *α* is favored.

In Figure 6b, it is observed that the intensity of the peaks (for steps 6 and 7) indicated as $\alpha\text{-}(110)_{PBA}$ and $\alpha\text{-}(020)_{PBA}$ increases (also see Figure 6d and Figures S15b and c). The absence of

peaks in the position of the *β-(020)* peak (see Figure 6c) suggests that the *β*-PBA is no longer present. Additionally, Figure 6d shows a decrease in the *d*-spacing, and an increase of the intensity that signals the *β*-*α* transformation. The curve at 24 °C, in Figure 6c, shows a combination of PBS-rich and the *α*-PBA-rich crystals. Therefore, the SSA protocol promotes the *β*-*α* change in the polymorphic forms of the PBA crystals.

The change from the *β* to the *α*-PBA phase is related to a perfecting process of the PBA unit cell at the lowest T_s. Doi et al.[74] describe this process in the annealing of PBA homopolymers. They claim that the first step of this transformation is the thickening of the *β*-PBA, in which the defects on the chain-folded surfaces are displaced, allowing a partial crystallization. Then, the *β* to *α* solid-solid transformation takes place, because the chains in the *β* crystal lattice acquire enough energy to change their conformation to that of the *α* crystals.[74] Recently, Wang et al.[86] found that a direct *β* to *α* transformation does not occur, and the change happens in two stages instead. First, the *β*-phase melts, and subsequently, the recrystallization of the amorphous phase leads to the *α*-phase. In another work, Cao and Wang also support a melt-recrystallization process.[87]

The *β* to *α* transformation occurs not only in the 40:60 PBSA, but also in the 20:80 PBSA when the SSA protocol is applied.

In the next section, we compare the changes caused by the crystallization conditions in the comonomer exclusion/inclusion balance and polymorphism in the PBSA random copolymers.

3.4. Comparison of the crystallization conditions at the pseudo-eutectic behavior and counit inclusion/exclusion balance in PBSA copolymers.

We have used three different crystallization conditions, and they displayed different behaviors that reflect changes in the pseudo-eutectic region and in the comonomer exclusion/inclusion balance. In this section, we compare and discuss these changes in the thermal and structural properties.

3.4.1. d-spacing analysis: comonomer inclusion

One of the most important indirect evidences of comonomer inclusion is given by the changes experienced in WAXS *d*-spacings of crystallographic planes, as comonomer composition varies. In this section, we discuss the differences in *d*-spacing generated by each crystallization condition.

Figure 7 shows how the *d*-spacing changes as a function of the BA content for isothermal (*i.e.*, low (Figure 7a) and high (Figure 7b) T_c) and SSA (Figure 7c) conditions.

PBS-rich compositions

Figures 7a and b show that the *d*-spacings of the PBS-rich phase crystals (80:20 and 60:40 PBSA copolymer compositions) remain almost unchanged, independently of the T_c values, as the BA content increases. Only high contents of BA counits (*i.e.*, 50 and 60%) change the *d*-spacing of the PBS-rich phase crystals, reflecting a higher BA inclusion in comparison with copolymers with low BA contents. The spacing of *(020)* PBS plane is more influenced by the BA inclusion as compared to the spacing of (*110)* PBS plane.

On the other hand, SSA experiments generate changes in *d*-spacing (see Figure 7c) for all PBS-rich compositions (from 20 to 60% BA contents). In this case, the increase of the *d*-spacing occurs

for both the *(110)* and *(020)* PBS planes, although the change is significantly larger for the *(020)* PBS crystalline planes. Such a trend in the entire composition range reflects a different extent of counit inclusion in comparison to isothermal experiments (and also non-isothermal, see Figure S16 in the SI).

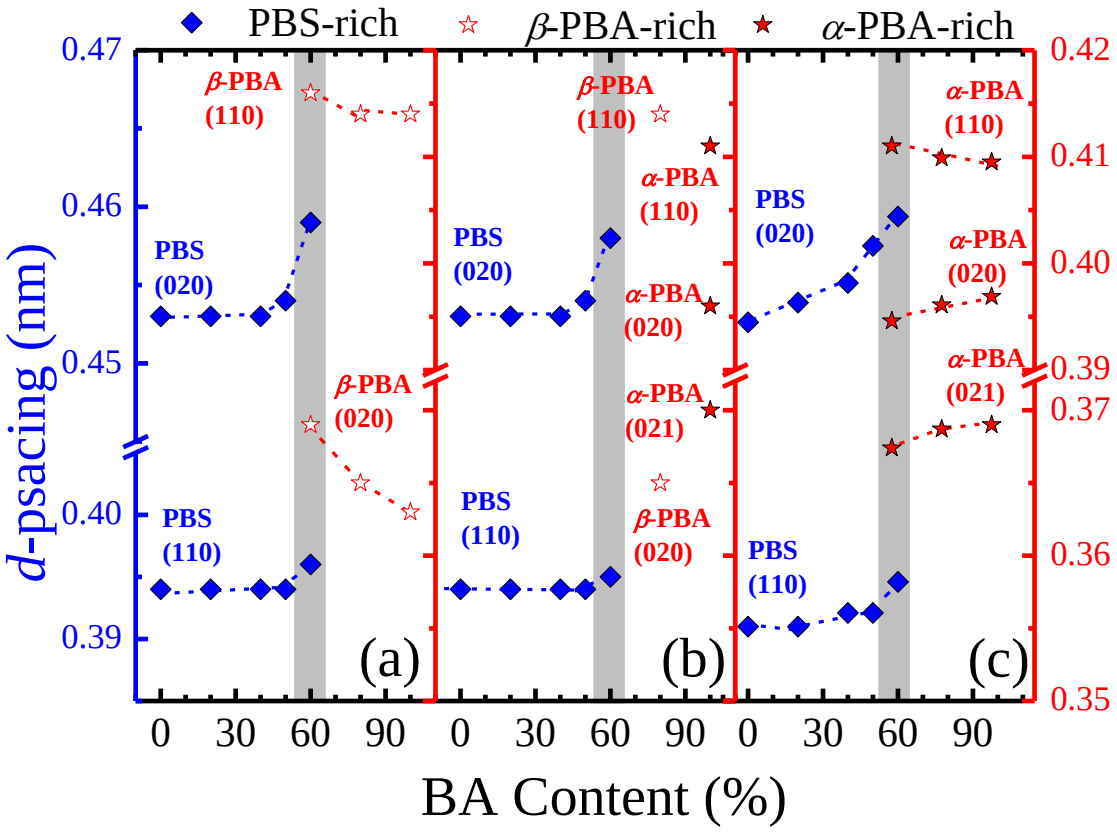

Figure 7. WAXS *d*-spacing as a function of BA content in the copolymers for (a,b) isothermal and (c) SSA experiments. Note that the left *y*-axis corresponds to the PBS and PBS-rich phase crystals *d*-spacing and the right *y*-axis to the PBA and PBA-rich phase crystals *d*-spacing. The isothermal results are divided into (a) low T_c (Figure 3a), and (b) high (Figure 3b) T_c values. In (c) we take the same crystal plane reflections for PBA$_{020}$ and PBS$_{110}$ for the 40:60 composition (see Figure 5) for comparison. Note that this peak has the contributions of both PBA and PBS crystal phases. We indicated the diffracted planes in brackets. The shadowed region corresponds to the pseudo-

eutectic region (*i.e.*, around the 40:60 PBSA composition). Note that in (c) the differences in *d*-spacing are only related to the composition, since the temperatures at which the WAXS pattern were measured do not have a significant influence.

Pseudo-eutectic region

The highest *d*-spacing changes occur near or at the pseudo-eutectic region (see shadow regions in Figure 7). For the PBS-rich phase crystals, the *d-spacings* corresponding to both *(110)* and *(020)* planes increase, as BA content increases, and have their maximum values at 60% BA content. This increase is related to the BA comonomer inclusion, especially significant for the 50:50 and 40:60 compositions. In the case of isothermal tests, the higher inclusion for these pseudo-eutectic compositions help explain the largest changes observed in the $1/\tau_{50\%}$ data, in comparison to the compositions containing less inclusion (lower BA content compositions), see Figure 1a.

We also found that in the 40:60 PBSA (*i.e.*, 60% BA content), at low T_c (see Figure 7a), both PBS-rich and PBA-rich phase crystals were formed; therefore, we could measure the *d*-spacings related to each phase. Such behavior was also observed in the SSA experiments (see Figure 7c). In contrast, in the isothermal crystallization experiments performed at high T_c (see Figure 7b), only PBS-rich phase crystals were formed in this 40:60 PBSA copolymer (i.e., 60% BA content).

PBA-rich compositions

In the PBA-rich regions in Figure 7, the changes in *d*-spacings are complex to analyze, due to the polymorphic nature of the PBA-rich phase crystals. At low T_c (Figure 7a), the *d*-spacings increase with BS content, practically in the entire composition range, evidencing BS inclusion (in

particular for the *(020)* planes the changes are significant). But, at high T_c (Figure 7b), the possible inclusion of BS units in the PBA-rich phase crystalline lattice, is difficult to judge since neat PBA crystallizes in the *α*-PBA phase, whereas the copolymers crystallize in the *β*-PBA phase.

Interestingly, the SSA experiments favor the formation of the more stable *α*-PBA crystalline phase (as shown in Figure 5), and the changes in *d*-spacings are different in comparison with those obtained for *β*-PBA phase crystals in isothermally crystallized samples (see Figures 7a and b). Figure 7c shows that only the *d*-spacing of the *(110) α*-PBA crystal plane shows an expansion upon increasing BS content. The *d*-spacings corresponding to the *(020)* and *(021)* planes show a decrease. We attribute this decrease to a compensation effect for the expansion of the unit cell along the *a* direction (see Section 3.4.2).

The decrease of the *d*-spacings in some *α*-PBA crystal planes might suggest a difficult BS inclusion in the *α*-PBA crystal lattice, in comparison with the *β*-PBA phase. Liang et al. [28] also found that *β*-PBA crystals better tolerate HA units inclusion rather than *α*-PBA crystals.

We discuss the different BS inclusion in the *α* and *β*-PBA phase (monoclinic vs. orthorhombic) in the next lines and in Section 3.4.2.

Normalized d-spacing comparisons

To further analyze the changes in WAXS *d*-spacings, we normalize them by the value of their respective homopolymer crystal, as *Normalized d*-spacing = (d-spacing$_{copolymer}$/d-spacing$_{homopolymer}$). These normalized spacings are plotted in Figure 8, as a function of the composition for each crystallization condition. The normalization of the *d*-spacings allows detecting their increases or decreases in comparison with those in the homopolymer unit cell (*i.e.*, PBS or PBA).

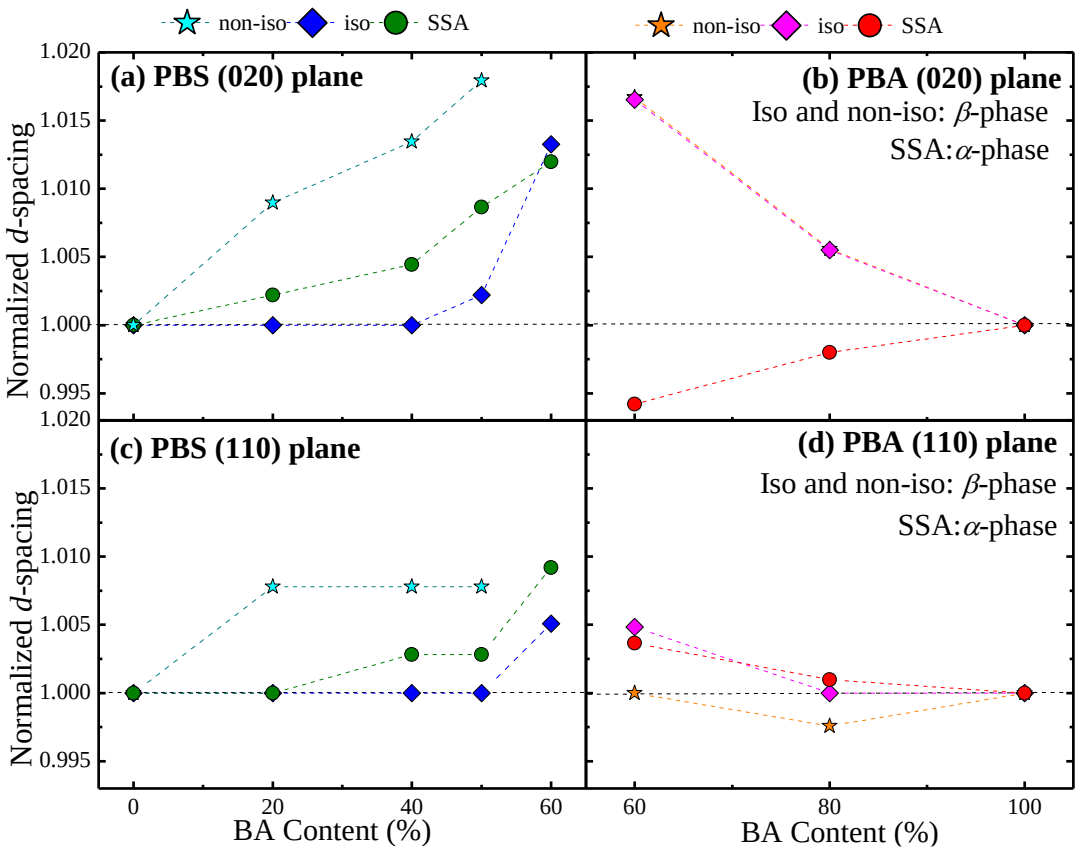

Figure 8. Normalized *d*-spacings for different crystallization conditions as a function of BA content. (a) PBS *(020)* plane, (b) PBA *(110)* plane, (c) PBS *(110)* plane and (d) PBA *(020)* plane. The data used for the PBS under non-isothermal test corresponds to cooling rates of 5 °C/min. In contrast, for comparison purposes, we have selected cooling rates of 50 °C/min instead for the neat PBA and its copolymers (in this condition, these materials crystallize in the *β*-PBA form) (see Figure S16). Note that the isothermal values correspond to low T_c conditions.

Figures 8a and c show how the PBS-rich crystal phase plane spacings increase as BA content increases. The magnitude of the increase in the normalized *d-spacings* depends on the crystallization conditions. The larger increases (*i.e.*, higher amount of BA comonomer inclusion

within the PBS-rich crystal phase) with BA content occur in the non-isothermally crystallized samples, followed by the SSA fractionated ones and, finally, by the isothermally crystallized. The maximum comonomer exclusion obtained by fast cooling (50 ºC/min) is expected for kinetic reasons. However, the difference between isothermally crystallized and SSA fractionated samples is unexpected. In view of the thermal cyclic protocol involved in SSA, one would expect that molecular segregation would also favor comonomeric exclusion. Nevertheless, the results of Figure 8 indicate that when the samples are crystallized isothermally, the degree of comonomer exclusion is higher.

One possible explanation is that SSA combines non-isothermal with isothermal steps. Hence, it is possible that during the non-isothermal crystallization steps, BA comonomeric units are included within the crystals in such a way that the subsequent annealing steps (during the 5 min isothermal holding times at T_s) are not able to completely exclude them. Hence, the result obtained is an exclusion/inclusion balance that is intermediate in between isothermal and non-isothermal crystallization.

In the non-isothermal experiments, the fast solidification traps more BA comonomer units inside the PBS-rich phase crystal unit cells, in comparison with an isothermal crystallization. Ruiz-Orta and Alamo[88] studied random propylene-*ran*-1-butene copolymers. They found that the fast crystallization favors the comonomer inclusion (*i.e.*, 1-butene) due to the minimized sequence selection; also, the faster crystallization hinders the molecular rearrangement needed for segregating comonomer into the amorphous phase.[89] In contrast, at a slow crystallization rate (*e.g.*, slow crystallization or isothermal crystallization at low supercooling) there is a crystallizable sequence selection, since the longer sequences are selected first, and the shorter sequences remain

in the surrounding residual melt. As a result, there are diffusion problems for these shorter sequences, since the long ones are already pinned to the crystal.[88]

The differences found in Figures 8a and 8c corroborate the findings of Ruiz-Orta and Alamo,[88] and suggest that the BA inclusion is higher in non-isothermally crystallized samples than in isothermally crystallized ones.

Figures 8b and 8d show the normalized *d-spacings* of the PBA-rich samples as a function of composition. In this case, the situation is different, because the crystallization conditions induce different PBA crystals polymorphic forms. Polymorphism is the crucial factor for determining comonomeric inclusion in the PBA-rich side of the composition diagram.

Figure 8b shows practically the same increase in *d*-spacing after applying a non-isothermal and isothermal test. According to our previous argument, the fast solidification during the non-isothermal test should lead to higher changes in the *d*-spacing than the isothermal test. However, we found similar changes in *d*-spacing, T_m (see Figures 2b and c), and X_c (see Figures S9a and b) values, suggesting that the comonomer inclusion in this case (*i.e.*, PBA rich phase crystals) is not sensitive to thermal history.

BS inclusion probably occurs in the PBA unit cells because the *d*-spacings values change with composition and also there are polymorphic changes which would not occur unless inclusion is present. In the current case, if the unit cell dimension is an indicator of the degree of inclusion, it seems that the BS-rich counits are "trapped" independently of the crystallization rate. A possible explanation is to consider that such BS inclusion inside the PBA unit cells is favored in such a way that the same amount of inclusion is obtained either by slow or fast cooling. We speculate that the inclusion of BS comonomeric units within the PBA unit cells is favored in comparison with BA

units in PBS crystal unit cells, as both α and β-PBA unit cell volumes are larger than that of the α-PBS unit cell.

Interestingly, Figure 8b and d show that the BS inclusion affects differently the α and β-PBA form. In the *(020)* PBA plane, there is an increase of the corresponding β-PBA values, and a decrease of the α-PBA values, as the BS content increases. In this case, a higher amount of BS inside the β-PBA crystals produces an expansion along the *b*-axis, whereas inside the α-PBA crystals the BS inclusion produces a compression.

For the *(110)* PBA plane, there is an increase of both α and β-PBA values as BS content increases, resulting in an expansion along the *a*-axis. The different changes in the α and β-PBA unit cell when the BS counits are included could also explain a distinct variation in the melting temperatures (Figure 2d) and crystallinities (Figure S9c) registered during the SSA experiments. To better understand these differences, we modeled the crystalline lattice of the parent components and the possible ways of inclusion of counits.

3.4.2. Inclusion models: Crystalline unit cell.

It is generally assumed that the expansion of the crystalline lattice reflects comonomer inclusion.[26] The reason for such expansion is related to the geometrical and energetic mismatch caused by comonomer inclusion. Although the conformation and packing of the comonomers inside the parent unit cells are unknown, we think it is interesting to discuss the changes in the crystalline lattice caused by comonomer inclusion.

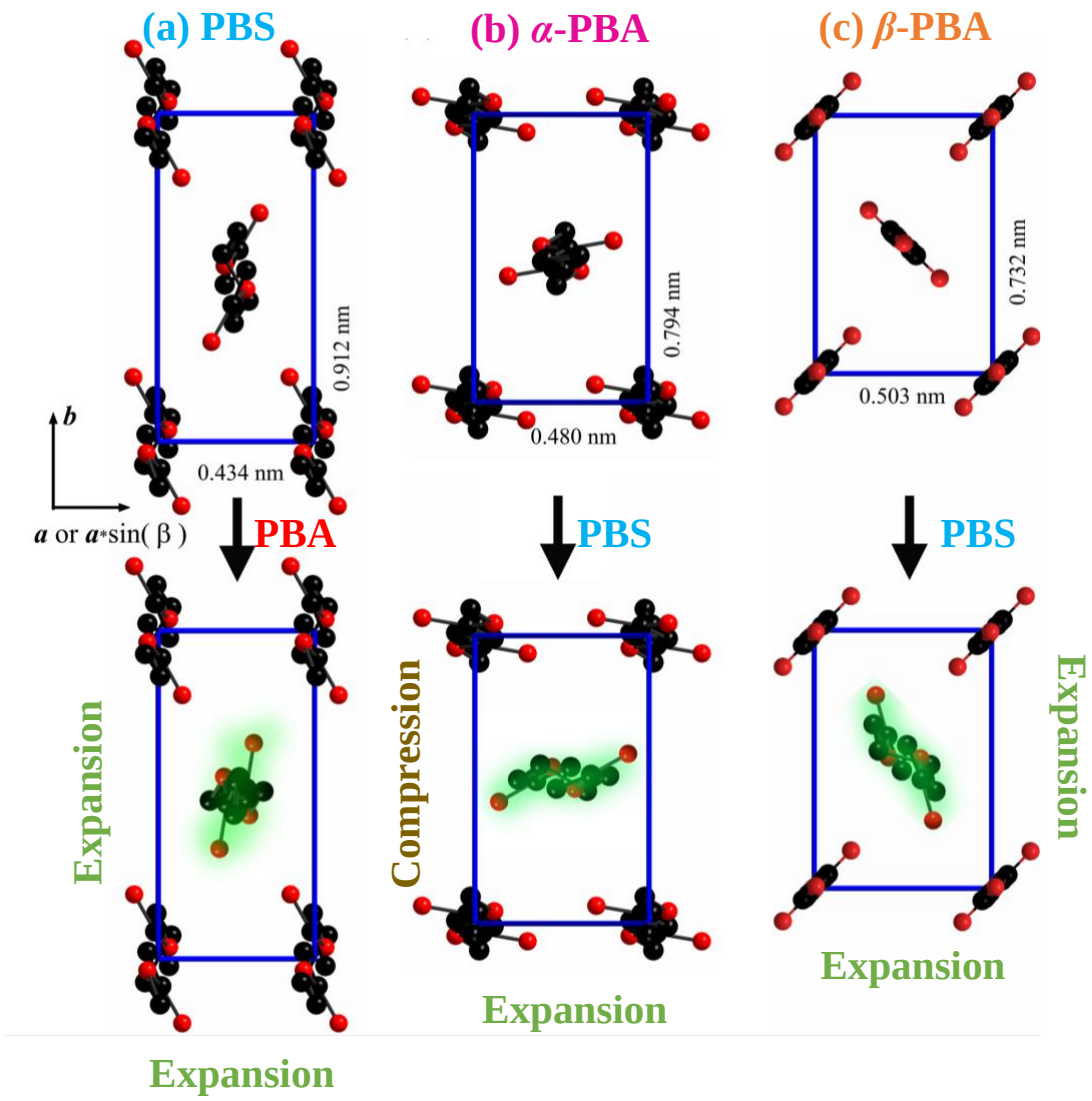

Figure 9. The unit cells for (a) PBS, (b) *α*-PBA, and (c) *β*-PBA projected along the *c*-axis. The atomic coordinates are from the references [36, 80, 90]. Below are proposed unit cells with (a) BA inclusion (*i.e.*, assuming the *α*-PBA form), (b) and (c) BS inclusion. The changes in the modeled unit cells are indicated.

The projections along the *c*-axis of different crystalline structures, including α-PBS, and β-PBA, are shown in Figure 9. We have employed the following values: *a*=0.523 nm, *b*=0.912 nm, *c*=1.090 nm (fiber axis), and β=123.98$_0$ for the α-PBS;[36] *a*=0.673 nm, *b*=0.794 nm, *c*=1.42 nm, and β=45.5$_0$ for the α-PBA;[80] and *a*=0.503 nm, *b*=0.732 nm, and *c*=1.442 nm (fiber axis) for the β-PBA.[90] The PBS and α-PBA crystallize in a monoclinic unit cell, while β-PBA has an orthorhombic unit cell. According to the above parameters, it is possible to calculate the cross-section (*A*) of each chain within the unit cell with Equation 1:

$$\mathrm{A} = b * a * \sin(\beta)/2 \qquad (1)$$

We found that PBS has a cross-section of 0.198 nm, comparable to that of α-PBA (0.191 nm) and higher than that of β-PBA (0.184 nm).

The top images of Figure 9 show the projection along the *c*-axis of the unit cells of the different parent components. For BA comonomer inclusion, although the conformation of the BA unit can be that of α or β phase, it seems that the general rule that a foreign comonomer (BA) expands the parent unit cell (BS) is fulfilled.

On the other hand, we have modeled the BS inclusion into the PBA unit cell, assuming that the BS units maintain the same conformation as in its homopolymer crystal when it enters into the PBA unit cell. We can notice that the BS chain is "thinner" and "longer" than the PBA chains in the α-crystals. Intuitively, it is reasonable to expect that the unit cell of α-PBA would shrink along the *b*-axis and expand along the *a*-axis (see the highlighted chain in the bottom of Figure 9b) to allow the BS unit inclusion. We observed this behavior in Figures 7c and 8b when the *d*-spacing corresponding to the *(020)* plane decreased.

In the case of the *β*-PBA, according to Figure 9, both *a* and *b*-axis might expand since the BS chain is much "bulkier" (*i.e.*, it has a larger cross-section) than the *zigzag* conformation of BA units in *β*-form (see the highlighted part in the bottom part of Figure 9c). We found evidence of this behavior in Figures 7a and 8d, in which the *d*-spacings corresponding to the *(110)* and *(020)* planes show an increase. This simple illustration corroborates our experimental finding pointing towards the role of polymorphic structure in comonomer inclusion for PBSA copolymers.

4. CONCLUSIONS

We studied the influence of the crystallization conditions on the comonomer exclusion/inclusion balance for biodegradable PBSA random copolymers. The explored crystallization conditions were non-isothermal, isothermal, and Successive Self-nucleation and Annealing (SSA).

Fast crystallization (*i.e.*, non-isothermal tests) favors BA inclusion inside the PBS phase crystals, whereas slow crystallization (*i.e.*, isothermal test) strongly limits it. The combination of fast and slow crystallization (*i.e.*, SSA test), investigated for the first time, generates an intermediate behavior, due to the inclusion of BA comonomers during the conditioning step, whereas the annealing steps allow less incorporation.

For what concerns PBA, both fast and slow crystallization formed the *β*-phase, indicating that BS unit inclusion is favored independently of the cooling conditions. A detailed study of polymorphic evolution of a PBA copolymer during SSA tests demonstrates that the sample initially crystallizes in the *β*-PBA phase but gradually changes to the more stable *α*-PBA as fractionation progresses.

PBS crystal unit cell expands to accommodate BA comonomeric unit inclusion. On the one hand, BS inclusion provokes an expansion of the *β*-PBA unit cell in the *a* and *b*-axis directions. On the

other hand, a combination of expansion in the *b*-axis and shrinkage in the *a*-axis occurs in the *α*-PBA unit cells to accommodate BS comonomeric units inside them. A simple crystallographic model has been proposed here to explain the changes in the unit cell dimension of the copolymers.

ASSOCIATED CONTENT

Supporting Information

The Supporting information provides further information of the SN, and SSA protocols and a brief description of the Hoffman-Weeks extrapolation, Lauritzen and Hoffman theory, and Flory and Baur models. We also include additional DSC and X-rays results.

AUTHOR INFORMATION

Corresponding Authors

Gouming Liu- Beijing National Laboratory for Molecular Sciences, CAS Key Laboratory of Engineering Plastics, CAS Research/Education Center for Excellence in Molecular Sciences, Institute of Chemistry, Chinese Academy of Sciences, Beijing 100190, China. University of Chinese Academy of Sciences, Beijing 100049, China. **orcid.org/0000-0003-2808-2661**

Email: gmliu@iccas.ac.cn

Alejandro J Müller- POLYMAT and Polymer Sciences and Technology Department, Faculty of Chemistry, University of the Basque Country UPV/EHU, Paseo Manuel de Lardizabal 3, 20018 Donostia-San Sebastián, Spain. IKERBASQUE, Basque Foundation for Science, 48013, Bilbao, Spain. **orcid.org/0000-0001-7009-7715**

Email: alejandrojesus.muller@ehu.es

Authors

Ricardo Arpad Pérez-Camargo-Beijing National Laboratory for Molecular Sciences, CAS Key Laboratory of Engineering Plastics, CAS Research/Education Center for Excellence in Molecular Sciences, Institute of Chemistry, Chinese Academy of Sciences, Beijing 100190, China; **orcid.org/0000-0003-4500-530X**

Dario Cavallo- Department of Chemistry and Industrial Chemistry, University of Genova, Genova, Italy.**orcid.org/0000-0002-3274-7067**

Dujin Wang-Beijing National Laboratory for Molecular Sciences, CAS Key Laboratory of Engineering Plastics, CAS Research/Education Center for Excellence in Molecular Sciences, Institute of Chemistry, Chinese Academy of Sciences, Beijing 100190, China. University of Chinese Academy of Sciences, Beijing 100049, China. **orcid.org/0000-0002-2063-0873**

Author Contributions

The manuscript was written through contributions of all authors. All authors have given approval to the final version of the manuscript.

Notes

The authors declare no competing financial interest.

ACKNOWLEDGMENTS

This work is supported by the National Key R&D Program of China (2017YFE0117800) and the National Natural Science Foundation of China (51820105005). R.A.P-C is supported by PIFI of the Chinese Academy of Science for international postdoctoral researchers (2019PE0004). This project has received funding from the European Union's Horizon 2020 research and innovation

program under the Marie Skłodowska-Curie grant agreement No 778092. This work has also received funding from MINECO through project MAT2017-83014-C2-1-P and from the Basque Government through grant IT1309-19.

We also thank Thibaud Debuissy and Luc Averous for providing us with the PBSA samples, whose synthesis has been reported in previous publications.[19, 91, 92] The support of the European Synchrotron Radiation Facility (ESRF) and the ALBA synchrotron facility is gratefully acknowledged.

5. REFERENCES

1. Sisti, L.; Totaro, G.; Marchese, P., PBS Makes its Entrance into the Family of Biobased Plastics. In *Biodegradable and Biobased Polymers for Environmental and Biomedical Applications*, Kalia, S.; Avérous, L., Eds. 2016; pp 225-285.

2. Papageorgiou, G. Z.; Papageorgiou, D. G., Solid-state structure and thermal characteristics of a sustainable biobased copolymer: Poly(butylene succinate-co-furanoate). *Thermochim. Acta* **2017,** 656, 112-122.

3. Terzopoulou, Z. N.; Papageorgiou, G. Z.; Papadopoulou, E.; Athanassiadou, E.; Alexopoulou, E.; Bikiaris, D. N., Green composites prepared from aliphatic polyesters and bast fibers. *Ind. Crops Prod.* **2015,** 68, 60-79.

4. Terzopoulou, Z. N.; Papageorgiou, G. Z.; Papadopoulou, E.; Athanassiadou, E.; Reinders, M.; Bikiaris, D. N., Development and study of fully biodegradable composite materials based on poly(butylene succinate) and hemp fibers or hemp shives. *Polym. Compos.* **2016,** 37, (2), 407-421.

5. Papageorgiou, G. Z.; Papageorgiou, D. G.; Chrissafis, K.; Bikiaris, D.; Will, J.; Hoppe, A.; Roether, J. A.; Boccaccini, A. R., Crystallization and Melting Behavior of Poly(Butylene Succinate) Nanocomposites Containing Silica-Nanotubes and Strontium Hydroxyapatite Nanorods. *Ind. Eng. Chem. Res.* **2014,** 53, (2), 678-692.

6. Guidotti, G.; Soccio, M.; Siracusa, V.; Gazzano, M.; Salatelli, E.; Munari, A.; Lotti, N., Novel Random PBS-Based Copolymers Containing Aliphatic Side Chains for Sustainable Flexible Food Packaging. *Polymers* **2017,** 9, (12), 724.

7. Genovese, L.; Lotti, N.; Gazzano, M.; Siracusa, V.; Dalla Rosa, M.; Munari, A., Novel biodegradable aliphatic copolyesters based on poly(butylene succinate) containing thioether-linkages for sustainable food packaging applications. *Polym. Degrad. Stab.* **2016,** 132, 191-201.

8. Arandia, I.; Zaldua, N.; Maiz, J.; Pérez-Camargo, R. A.; Mugica, A.; Zubitur, M.; Mincheva, R.; Dubois, P.; Müller, A. J., Tailoring the isothermal crystallization kinetics of isodimorphic poly (butylene succinate-ran-butylene azelate) random copolymers by changing composition. *Polymer* **2019,** 183, 121863.

9. Pérez-Camargo, R. A.; Arandia, I.; Safari, M.; Cavallo, D.; Lotti, N.; Soccio, M.; Müller, A. J., Crystallization of isodimorphic aliphatic random copolyesters: Pseudo-eutectic behavior and double-crystalline materials. *Eur. Polym. J.* **2018,** 101, 233-247.

10. Yu, Y.; Sang, L.; Wei, Z.; Leng, X.; Li, Y., Unique isodimorphism and isomorphism behaviors of even-odd poly(hexamethylene dicarboxylate) aliphatic copolyesters. *Polymer* **2017,** 115, 106-117.

11. Latere Dwan'Isa, J.-P.; Lecomte, P.; Dubois, P.; Jérôme, R., Synthesis and Characterization of Random Copolyesters of ε-Caprolactone and 2-Oxepane-1,5-dione. *Macromolecules* **2003,** 36, (8), 2609-2615.

12. Ceccorulli, G.; Scandola, M.; Kumar, A.; Kalra, B.; Gross, R. A., Cocrystallization of Random Copolymers of ω-Pentadecalactone and ε-Caprolactone Synthesized by Lipase Catalysis. *Biomacromolecules* **2005,** 6, (2), 902-907.

13. Ye, H.-M.; Wang, R.-D.; Liu, J.; Xu, J.; Guo, B.-H., Isomorphism in Poly(butylene succinate-co-butylene fumarate) and Its Application as Polymeric Nucleating Agent for Poly(butylene succinate). *Macromolecules* **2012,** 45, (14), 5667-5675.

14. Basterretxea, A.; Gabirondo, E.; Flores, I.; Etxeberria, A.; Gonzalez, A.; Müller, A. J.; Mecerreyes, D.; Coulembier, O.; Sardon, H., Isomorphic Polyoxyalkylene Copolyethers Obtained by Copolymerization of Aliphatic Diols. *Macromolecules* **2019,** 52, (9), 3506-3515.

15. Arandia, I.; Meabe, L.; Aranburu, N.; Sardon, H.; Mecerreyes, D.; Müller, A. J., Influence of Chemical Structures on Isodimorphic Behavior of Three Different Copolycarbonate Random Copolymer Series. *Macromolecules* **2020**, 53, (2), 669-681.

16. Arandia, I.; Mugica, A.; Zubitur, M.; Arbe, A.; Liu, G.; Wang, D.; Mincheva, R.; Dubois, P.; Müller, A. J., How Composition Determines the Properties of Isodimorphic Poly(butylene succinate-ran-butylene azelate) Random Biobased Copolymers: From Single to Double Crystalline Random Copolymers. *Macromolecules* **2015,** 48, (1), 43-57.

17. Arandia, I.; Mugica, A.; Zubitur, M.; Iturrospe, A.; Arbe, A.; Liu, G.; Wang, D.; Mincheva, R.; Dubois, P.; Müller, A. J., Application of SSA thermal fractionation and X-ray diffraction to

elucidate comonomer inclusion or exclusion from the crystalline phases in poly(butylene succinate-ran-butylene azelate) random copolymers. *J. Polym. Sci., Part B: Polym. Phys.* **2016,** 54, (22), 2346-2358.

18. Arandia, I.; Mugica, A.; Zubitur, M.; Mincheva, R.; Dubois, P.; Müller, A. J.; Alegría, A., The Complex Amorphous Phase in Poly(butylene succinate-ran-butylene azelate) Isodimorphic Copolyesters. *Macromolecules* **2017,** 50, (4), 1569-1578.

19. Pérez-Camargo, R. A.; Fernández-d'Arlas, B.; Cavallo, D.; Debuissy, T.; Pollet, E.; Avérous, L.; Müller, A. J., Tailoring the Structure, Morphology, and Crystallization of Isodimorphic Poly(butylene succinate-ran-butylene adipate) Random Copolymers by Changing Composition and Thermal History. *Macromolecules* **2017,** 50, (2), 597-608.

20. Ciulik, C.; Safari, M.; Martínez de Ilarduya, A.; Morales-Huerta, J. C.; Iturrospe, A.; Arbe, A.; Müller, A. J.; Muñoz-Guerra, S., Poly(butylene succinate-ran-ε-caprolactone) copolyesters: Enzymatic synthesis and crystalline isodimorphic character. *Eur. Polym. J.* **2017,** 95, 795-808.

21. Safari, M.; Martínez De Ilarduya, A.; Mugica, A.; Zubitur, M.; Muñoz-Guerra, S.; Müller, A. J., Tuning the Thermal Properties and Morphology of Isodimorphic Poly[(butylene succinate)-ran-(ϵ-caprolactone)] Copolyesters by Changing Composition, Molecular Weight, and Thermal History. *Macromolecules* **2018,** 51, (23), 9589-9601.

22. Safari, M.; Mugica, A.; Zubitur, M.; Martínez de Ilarduya, A.; Muñoz-Guerra, S.; Müller, A. J., Controlling the Isothermal Crystallization of Isodimorphic PBS-ran-PCL Random Copolymers by Varying Composition and Supercooling. *Polymers* **2019,** 12, (1), 17.

23. Yu, Y.; Wei, Z.; Zheng, L.; Jin, C.; Leng, X.; Li, Y., Competition and miscibility of isodimorphism and their effects on band spherulites and mechanical properties of poly(butylene succinate-co-cis-butene succinate) unsaturated aliphatic copolyesters. *Polymer* **2018,** 150, 52-63.

24. Yu, Y.; Wei, Z.; Liu, Y.; Hua, Z.; Leng, X.; Li, Y., Effect of chain length of comonomeric diols on competition and miscibility of isodimorphism: A comparative study of poly(butylene glutarate-co-butylene azelate) and poly(octylene glutarate-co-octylene azelate). *Eur. Polym. J.* **2018,** 105, 274-285.

25. Thalladi, V. R.; Boese, R.; Weiss, H.-C., The Melting Point Alternation in α,ω-Alkanedithiols. *J. Am. Chem. Soc.* **2000,** 122, (6), 1186-1190.

26. Mandelkern, L., *Crystallization of Polymers: Volume 1: Equilibrium Concepts*. 2 ed.; Cambridge University Press: Cambridge, 2002; Vol. 1.

27. Liang, Z.; Pan, P.; Zhu, B.; Inoue, Y., Isomorphic crystallization of aliphatic copolyesters derived from 1,6-hexanediol: Effect of the chemical structure of comonomer units on the extent of cocrystallization. *Polymer* **2011,** 52, (12), 2667-2676.

28. Liang, Z.; Pan, P.; Zhu, B.; Inoue, Y., Isomorphic Crystallization of Poly(hexamethylene adipate-co-butylene adipate): Regulating Crystal Modification of Polymorphic Polyester from Internal Crystalline Lattice. *Macromolecules* **2010,** 43, (15), 6429-6437.

29. Pan, P.; Inoue, Y., Polymorphism and isomorphism in biodegradable polyesters. *Prog. Polym. Sci.* **2009,** 34, (7), 605-640.

30. Flory, P. J., Thermodynamics of Crystallization in High Polymers II. Simplified Derivation of Melting-Point Relationships. *J. Chem. Phys.* **1947,** 15, (9), 684-684.

31. Baur, V. H., Einfluß der sequenzlängenverteilung auf das schmelz-ende von copolymeren. *Makromol. Chem.* **1966,** 98, (1), 297-301.

32. Sanchez, I. C.; Eby, R. K., Thermodynamics and Crystallization of Random Copolymers. *Macromolecules* **1975,** 8, (5), 638-641.

33. Wendling, J.; Suter, U. W., A New Model Describing the Cocrystallization Behavior of Random Copolymers. *Macromolecules* **1998,** 31, (8), 2516-2520.

34. Ren, M.; Song, J.; Song, C.; Zhang, H.; Sun, X.; Chen, Q.; Zhang, H.; Mo, Z., Crystallization kinetics and morphology of poly(butylene succinate-co-adipate). *J. Polym. Sci., Part B: Polym. Phys.* **2005,** 43, (22), 3231-3241.

35. Ichikawa, Y.; Suzuki, J.; Washiyama, J.; Moteki, Y.; Noguchi, K.; Okuyama, K., Strain-induced crystal modification in poly(tetramethylene succinate). *Polymer* **1994,** 35, (15), 3338-3339.

36. Ichikawa, Y.; Kondo, H.; Igarashi, Y.; Noguchi, K.; Okuyama, K.; Washiyama, J., Crystal structures of α and β forms of poly(tetramethylene succinate). *Polymer* **2000,** 41, (12), 4719-4727.

37. Siracusa, V.; Lotti, N.; Munari, A.; Dalla Rosa, M., Poly(butylene succinate) and poly(butylene succinate-co-adipate) for food packaging applications: Gas barrier properties after stressed treatments. *Polym. Degrad. Stab.* **2015,** 119, 35-45.

38. Nikolic, M. S.; Djonlagic, J., Synthesis and characterization of biodegradable poly(butylene succinate-co-butylene adipate)s. *Polym. Degrad. Stab.* **2001,** 74, (2), 263-270.

39. Gigli, M.; Negroni, A.; Zanaroli, G.; Lotti, N.; Fava, F.; Munari, A., Environmentally friendly PBS-based copolyesters containing PEG-like subunit: Effect of block length on solid-state properties and enzymatic degradation. *React. Funct. Polym.* **2013,** 73, (5), 764-771.

40. Tokiwa, Y.; Calabia, B. P., Biodegradability and Biodegradation of Polyesters. *J. Polym. Environ.* **2007,** 15, (4), 259-267.

41. Puchalski, M.; Szparaga, G.; Biela, T.; Gutowska, A.; Sztajnowski, S.; Krucińska, I., Molecular and supramolecular changes in polybutylene succinate (PBS) and polybutylene succinate adipate (PBSA) copolymer during degradation in various environmental conditions. *Polymers* **2018,** 10, (3), 251.

42. Hemashenpagam, N.; Growther, L.; Murgalatha, N.; Vasantha Raj, S.; Sathiya Vimal, S., Isolation and characterization of a bacterium that degrades PBSA. *Int. J. Pharm. Bio. Sci.* **2013,** 4, (4), B335-B342.

43. Quattrosoldi, S.; Soccio, M.; Gazzano, M.; Lotti, N.; Munari, A., Fully biobased, elastomeric and compostable random copolyesters of poly(butylene succinate) containing Pripol 1009 moieties: Structure-property relationship. *Polym. Degrad. Stab.* **2020,** 178, 109189.

44. Tserki, V.; Matzinos, P.; Pavlidou, E.; Vachliotis, D.; Panayiotou, C., Biodegradable aliphatic polyesters. Part I. Properties and biodegradation of poly(butylene succinate-co-butylene adipate). *Polym. Degrad. Stab.* **2006,** 91, (2), 367-376.

45. Tang, Y.-R.; Xu, J.; Guo, B.-H., Polymorphic Behavior and Enzymatic Degradation of Poly(butylene adipate) in the Presence of Hexagonal Boron Nitride Nanosheets. *Ind. Eng. Chem. Res.* **2015,** 54, (6), 1832-1841.

46. Hou, C.; Sun, X.; Ren, Z.; Li, H.; Yan, S., Polymorphism and Enzymatic Degradation of Poly(1,4-butylene adipate) and Its Binary Blends with Atactic Poly(3-hydroxybutyrate) and Poly(vinyl phenol). *Ind. Eng. Chem. Res.* **2017,** 56, (48), 14263-14269.

47. Gan, Z.; Kuwabara, K.; Abe, H.; Iwata, T.; Doi, Y., The role of polymorphic crystal structure and morphology in enzymatic degradation of melt-crystallized poly(butylene adipate) films. *Polym. Degrad. Stab.* **2005,** 87, (1), 191-199.

48. Yang, J.; Pan, P.; Hua, L.; Zhu, B.; Dong, T.; Inoue, Y., Polymorphic Crystallization and Phase Transition of Poly(butylene adipate) in Its Miscible Crystalline/Crystalline Blend with Poly(vinylidene fluoride). *Macromolecules* **2010,** 43, (20), 8610-8618.

49. Yang, J.; Pan, P.; Hua, L.; Feng, X.; Yue, J.; Ge, Y.; Inoue, Y., Effects of Crystallization Temperature of Poly(vinylidene fluoride) on Crystal Modification and Phase Transition of Poly(butylene adipate) in Their Blends: A Novel Approach for Polymorphic Control. *J. Phys. Chem. B.* **2012,** 116, (4), 1265-1272.

50. Liang, Z.; Yang, J.; Hua, L.; Pan, P.; Huang, J.; Zhang, J.; Abe, H.; Inoue, Y., Polymorphic crystallization of poly(butylene adipate) and its copolymer: Effect of poly(vinyl alcohol). *J. Appl. Polym. Sci.* **2014,** 131, (1), 39600.

51. Dong, T.; Kai, W.; Inoue, Y., Regulation of Polymorphic Behavior of Poly(butylene adipate) upon Complexation with α-Cyclodextrin. *Macromolecules* **2007,** 40, (23), 8285-8290.

52. Weng, M.; He, Y.; Qiu, Z., Effect of Uracil on the Isothermal Melt Crystallization Kinetics and Polymorphic Crystals Control of Biodegradable Poly(butylene adipate). *Ind. Eng. Chem. Res.* **2012,** 51, (42), 13862-13868.

53. Lorenzo, A. T.; Arnal, M. L.; Albuerne, J.; Müller, A. J., DSC isothermal polymer crystallization kinetics measurements and the use of the Avrami equation to fit the data: Guidelines to avoid common problems. *Polym. Test.* **2007,** 26, (2), 222-231.

54. Blundell, D. J.; Keller, A.; Kovacs, A. J., A new self-nucleation phenomenon and its application to the growing of polymer crystals from solution. *J. Polym. Sci., Part B: Polym. Lett.* **1966,** 4, (7), 481-486.

55. Fillon, B.; Wittmann, J. C.; Lotz, B.; Thierry, A., Self-nucleation and recrystallization of isotactic polypropylene (α phase) investigated by differential scanning calorimetry. *J. Polym. Sci., Part B: Polym. Phys.* **1993,** 31, (10), 1383-1393.

56. Michell, R. M.; Mugica, A.; Zubitur, M.; Müller, A. J., Self-Nucleation of Crystalline Phases Within Homopolymers, Polymer Blends, Copolymers, and Nanocomposites. In *Polymer Crystallization I: From Chain Microstructure to Processing*, Auriemma, F.; Alfonso, G. C.; de Rosa, C., Eds. Springer International Publishing: Cham, 2017; pp 215-256.

57. Lorenzo, A. T.; Arnal, M. L.; Müller, A. J.; Boschetti de Fierro, A.; Abetz, V., High Speed SSA Thermal Fractionation and Limitations to the Determination of Lamellar Sizes and Their Distributions. *Macromol. Chem. Phys.* **2006,** 207, (1), 39-49.

58. Müller, A. J.; Arnal, M. L., Thermal fractionation of polymers. *Prog. Polym. Sci.* **2005,** 30, (5), 559-603.

59. Müller, A. J.; Hernández, Z. H.; Arnal, M. L.; Sánchez, J. J., Successive self-nucleation/annealing (SSA): A novel technique to study molecular segregation during crystallization. *Polym. Bull.* **1997,** 39, (4), 465-472.

60. Müller, A. J.; Michell, R. M.; Pérez, R. A.; Lorenzo, A. T., Successive Self-nucleation and Annealing (SSA): Correct design of thermal protocol and applications. *Eur. Polym. J.* **2015,** 65, 132-154.

61. Lorenzo, A. T.; Arnal, M. L.; Müller, A. J.; Lin, M.-C.; Chen, H.-L., SAXS/DSC Analysis of the Lamellar Thickness Distribution on a SSA Thermally Fractionated Model Polyethylene. *Macromol. Chem. Phys.* **2011,** 212, (18), 2009-2016.

62. Müller, A. J.; Lorenzo, A. T.; Arnal, M. L., Recent Advances and Applications of "Successive Self-Nucleation and Annealing" (SSA) High Speed Thermal Fractionation. *Macromol. Symp.* **2009,** 277, (1), 207-214.

63. Lauritzen, J. I.; Hoffman, J. D., Theory of Formation of Polymer Crystals with Folded Chains in Dilute Solution. *J. Res. Natl. Bur. Stand., Sect. A* **1960,** 64A, (1), 73-102.

64. Hoffman, J. D.; Lauritzen, J. I., Crystallization of Bulk Polymers With Chain Folding: Theory of Growth of Lamellar Spherulites *J. Res. Natl. Bur. Stand., Sect. A* **1961,** 65A, (4), 297-336.

65. Lorenzo, A. T.; Müller, A. J., Estimation of the nucleation and crystal growth contributions to the overall crystallization energy barrier. *J. Polym. Sci., Part B: Polym. Phys.* **2008,** 46, (14), 1478-1487.

66. Müller, A. J.; Albuerne, J.; Marquez, L.; Raquez, J.-M.; Degée, P.; Dubois, P.; Hobbs, J.; Hamley, I. W., Self-nucleation and crystallization kinetics of double crystalline poly(p-dioxanone)-b-poly(ε-caprolactone) diblock copolymers. *Faraday Discuss.* **2005,** 128, (0), 231-252.

67. Sabino, M. A.; Albuerne, J.; Müller, A. J.; Brisson, J.; Prud'homme, R. E., Influence of in Vitro Hydrolytic Degradation on the Morphology and Crystallization Behavior of Poly(p-dioxanone). *Biomacromolecules* **2004,** 5, (2), 358-370.

68. Lambert, W. S.; Phillips, P. J., Crystallization Kinetics of Low Molecular Weight Fractions of Branched Polyethylenes. *Macromolecules* **1994,** 27, (13), 3537-3542.

69. Lorenzo, A. T.; Arnal, M. L.; Müller, A. J.; Boschetti-de-Fierro, A.; Abetz, V., Nucleation and Isothermal Crystallization of the Polyethylene Block within Diblock Copolymers Containing Polystyrene and Poly(ethylene-alt-propylene). *Macromolecules* **2007,** 40, (14), 5023-5037.

70. Hoffman, J. D.; Weeks, J. J., Melting process and the equilibrium melting temperature of polychlorotrifluoroethylene. *J. Res. Natl. Bur. Stand. Sect. A* **1962,** 66A, (1), 13-28.

71. Gan, Z.; Abe, H.; Kurokawa, H.; Doi, Y., Solid-State Microstructures, Thermal Properties, and Crystallization of Biodegradable Poly(butylene succinate) (PBS) and Its Copolyesters. *Biomacromolecules* **2001,** 2, (2), 605-613.

72. Miyata, T.; Masuko, T., Crystallization behaviour of poly(tetramethylene succinate). *Polymer* **1998,** 39, (6), 1399-1404.

73. Yoo, E. S.; Im, S. S., Melting behavior of poly(butylene succinate) during heating scan by DSC. *J. Polym. Sci., Part B: Polym. Phys.* **1999,** 37, (13), 1357-1366.

74. Gan, Z.; Kuwabara, K.; Abe, H.; Iwata, T.; Doi, Y., Metastability and Transformation of Polymorphic Crystals in Biodegradable Poly(butylene adipate). *Biomacromolecules* **2004,** 5, (2), 371-378.

75. Yamada, S.; Wang, Y.; Asakawa, N.; Yoshie, N.; Inoue, Y., Crystalline Structural Change of Bacterial Poly(3-hydroxybutyrate-co-3-hydroxyvalerate) with Narrow Compositional Distribution. *Macromolecules* **2001,** 34, (13), 4659-4661.

76. Yang, J.; Pan, P.; Hua, L.; Xie, Y.; Dong, T.; Zhu, B.; Inoue, Y.; Feng, X., Fractionated crystallization, polymorphic crystalline structure, and spherulite morphology of poly(butylene adipate) in its miscible blend with poly(butylene succinate). *Polymer* **2011,** 52, (15), 3460-3468.

77. Ye, H.-M.; Tang, Y.-R.; Xu, J.; Guo, B.-H., Role of Poly(butylene fumarate) on Crystallization Behavior of Poly(butylene succinate). *Ind. Eng. Chem. Res.* **2013,** 52, (31), 10682-10689.

78. Liu, G.; Zheng, L.; Zhang, X.; Li, C.; Wang, D., Critical Stress for Crystal Transition in Poly(butylene succinate)-Based Crystalline–Amorphous Multiblock Copolymers. *Macromolecules* **2014,** 47, (21), 7533-7539.

79. Liu, J.; Ye, H.-M.; Xu, J.; Guo, B.-H., Formation of ring-banded spherulites of α and β modifications in Poly(butylene adipate). *Polymer* **2011,** 52, (20), 4619-4630.

80. Pouget, E.; Almontassir, A.; Casas, M. T.; Puiggalí, J., On the Crystalline Structures of Poly(tetramethylene adipate). *Macromolecules* **2003,** 36, (3), 698-705.

81. Minke, R.; Blackwell, J., Single crystals of poly(tetramethylene adipate). *Journal of Macromolecular Science, Part B* **1980,** 18, (2), 233-255.

82. Lugito, G.; Woo, E. M., Intertwining lamellar assembly in porous spherulites composed of two ring-banded poly(ethylene adipate) and poly(butylene adipate). *Soft Matter* **2015,** 11, (5), 908-917.

83. Papageorgiou, G. Z.; Tsanaktsis, V.; Bikiaris, D. N., Crystallization of poly(butylene-2,6-naphthalate-co-butylene adipate) copolymers: regulating crystal modification of the polymorphic parent homopolymers and biodegradation. *CrystEngComm* **2014,** 16, (34), 7963-7978.

84. Gan, Z.; Abe, H.; Doi, Y., Temperature-Induced Polymorphic Crystals of Poly(butylene adipate). *Macromol. Chem. Phys.* **2002,** 203, (16), 2369-2374.

85. Woo, E. M.; Wu, M. C., Thermal and X-ray analysis of polymorphic crystals, melting, and crystalline transformation in poly(butylene adipate). *J. Polym. Sci. Part B:, Polym. Phys.* **2005,** 43, (13), 1662-1672.

86. Wang, M.; Tashiro, K.; Ozaki, Y., Reinvestigation of the β-to-α Crystal Phase Transition of Poly(butylene adipate) by the Time-Resolved X-ray Scattering and FTIR Spectral Measurements in the Temperature-Jump Process. *Macromolecules* **2017,** 50, (10), 3883-3889.

87. Wang, M.; Cao, W., Phase Transition and Melt-Recrystallization Behavior of Poly(Butylene Adipate) Investigated by Simultaneous Measurements of Wide-Angle X-Ray Diffraction (WAXD) and Differential Scanning Calorimetry (DSC). *Polymers* **2020,** 12, (1), 75.

88. Ruiz-Orta, C.; Alamo, R. G., Morphological and kinetic partitioning of comonomer in random propylene 1-butene copolymers. *Polymer* **2012,** 53, (3), 810-822.

89. Roe, R.-J.; Gieniewski, C., Partitioning of comonomer units between crystalline and amorphous phases of polyethylene: Effect of crystallization conditions. *J. Cryst. Growth* **1980,** 48, (2), 295-302.

90. Iwata, T.; Kobayashi, S.; Tabata, K.; Yonezawa, N.; Doi, Y., Crystal Structure, Thermal Behavior and Enzymatic Degradation of Poly(tetramethylene adipate) Solution-Grown Chain-Folded Lamellar Crystals. *Macromol. Biosci.* **2004,** 4, (3), 296-307.

91. Debuissy, T.; Pollet, E.; Avérous, L., Synthesis and characterization of biobased poly(butylene succinate-ran-butylene adipate). Analysis of the composition-dependent physicochemical properties. *Eur. Polym. J.* **2017,** 87, 84-98.

92. Debuissy, T.; Pollet, E.; Avérous, L., Synthesis of potentially biobased copolyesters based on adipic acid and butanediols: Kinetic study between 1,4- and 2,3-butanediol and their influence on crystallization and thermal properties. *Polymer* **2016,** 99, 204-213.

For graphical abstract only

Effect of the crystallization conditions on the exclusion/inclusion balance in biodegradable poly (butylene succinate-*ran*-butylene adipate) copolymers

Ricardo Arpad Pérez-Camargo[1], Guoming Liu[1,2], Dario Cavallo[3], Dujin Wang[1,2] and Alejandro J Müller[4,5]**